© 2021. Published by The Company of Biologists Ltd | Journal of Cell Science (2021) 134, jcs257535. doi:10.1242/jcs.257535

RESEARCH ARTICLE

The miR-26 family regulates neural differentiation-associated microRNAs and mRNAs by directly targeting REST

Mark Sauer[1,*], Nina Was[1,*], Thomas Ziegenhals[2], Xiantao Wang[3], Markus Hafner[3], Matthias Becker[1,‡] and Utz Fischer[2,‡]

ABSTRACT

Repressor element 1-silencing transcription factor (REST) plays a crucial role in the differentiation of neural progenitor cells (NPCs). C-terminal domain small phosphatases (CTDSPs) are REST effector proteins that reduce RNA polymerase II activity on genes required for neurogenesis. miR-26b regulates neurogenesis in zebrafish by targeting *ctdsp2* mRNA, but the molecular events triggered by this microRNA (miR) remain unknown. Here, we show in a murine embryonic stem cell differentiation paradigm that inactivation of miR-26 family members disrupts the formation of neurons and astroglia and arrests neurogenesis at the neural progenitor level. Furthermore, we show that miR-26 directly targets *Rest*, thereby inducing the expression of a large set of REST complex-repressed neuronal genes, including miRs required for induction of the neuronal gene expression program. Our data identify the miR-26 family as the trigger of a self-amplifying system required for neural differentiation that acts upstream of REST-controlled miRs.

KEY WORDS: REST, miR-26, MicroRNA, Neurogenesis, Neuronal differentiation

INTRODUCTION

The generation of the central nervous system (CNS) from progenitor cells is a precisely controlled and developmental stage-specific continuum. In vertebrates, this process starts with ectoderm differentiation, the regionalization of the CNS and neurulation. At the molecular level, neurogenesis requires the activation of a complex gene expression program that is suppressed in non-neuronal cells and in undifferentiated neural progenitor cells (NPCs). Suppression is achieved through the repressor element 1-silencing transcription factor (REST) complex (Ballas et al., 2005; Chen et al., 1998; Schoenherr and Anderson, 1995), which binds to genes containing repressor element 1 (RE1) in *cis* (Ballas et al., 2005). Binding of the REST complex enables the recruitment of an additional repressive complex containing REST corepressor 1 (CoREST). When recruited to RE1 elements, REST–CoREST can serve as a binding platform for various effector proteins that act on chromatin and on RNA polymerase II (Pol II) (Andres et al., 1999; Qureshi et al., 2010). Important effector proteins acting directly on Pol II transcription are carboxy-terminal domain (CTD) small phosphatase proteins (CTDSPs). These enzymes dephosphorylate the CTD of Pol II on RE1-controlled genes, thereby inhibiting its transcriptional activity. During neural fate commitment and terminal differentiation, the REST pathway is gradually inactivated to allow the expression of RE1-containing genes (Ballas et al., 2005; Yeo et al., 2005). Inactivation of REST and its effector proteins involves the action of various microRNAs (miRs). These include miR-9/miR-9*, which represses REST and CoREST; miR-124, which targets Ctdsp mRNAs; and miR-132, which represses the REST-associated chromatin factor MeCp2 (Conaco et al., 2006; Klein et al., 2007; Packer et al., 2008; Visvanathan et al., 2007). Interestingly, these miRs are all themselves under control of the RE1–REST axis and thus are part of a negative feedback loop (Conaco et al., 2006; Johnson et al., 2008; Packer et al., 2008; Wu and Xie, 2006). Therefore, an initial event is required during the differentiation of NPCs to neurons, which triggers REST inactivation and the induction of a neuron-specific gene expression program. Candidates for this task are members of the miR-26 family. In zebrafish, miR-26b binds to the *ctdsp2* mRNA, thereby repressing its own host, which supports neuronal differentiation (Dill et al., 2012; Han et al., 2012). In mammals, miR-26 family members are encoded in the introns of genes encoding CTDSPs (miR-26a1 in *CtdspL*, miR-26a2 in *Ctdsp2* and miR-26b in *Ctdsp1*). A role for miR-26 in the mammalian CNS *in vivo* and *in vitro* has previously been suggested (Ehses et al., 2020; Xie et al., 2019; Zhang et al., 2018). In contrast to these findings, miR-26-knockout (KO) mice display no obvious defects in brain development (Acharya et al., 2019; Sun et al., 2018; Zhang et al., 2017). Therefore, an as yet unknown mechanism may exist that compensates the *in vivo* function of miR-26 in neural development in mice.

In zebrafish, mature miR-26b is not constitutively co-expressed with its *ctdsp2* host, but rather is kept in an inactive form. This is most likely achieved through the inhibition of miR-26 processing in NPCs and in non-neuronal cells. Importantly, miR-26 is not controlled by, and hence may act independently of, the REST complex. This makes the miR-26 family a good candidate for being a key regulator of neuronal differentiation. To test this hypothesis, and to understand the molecular mechanism by which this miR family acts, we employed a cell culture system that allows the faithful differentiation of embryonic stem cells (ESCs) via NPCs to neural cells (NCs). We show that genomic deletion of the entire miR-26 family, or individual members thereof, does not interfere with the differentiation of ESCs into NPCs. However, the subsequent differentiation into NCs is severely affected. In accordance with this phenotypic observation, a transcriptome analysis revealed that the deletion of the miR-26 family members

[1]Institute for Medical Radiology and Cell Research (MSZ) in the Center for Experimental Molecular Medicine (ZEMM), University of Würzburg, D-97078 Würzburg, Germany. [2]Department of Biochemistry, Theodor Boveri-Institute, University of Würzburg, D-97074 Würzburg, Germany. [3]RNA Molecular Biology Group, Laboratory of Muscle Stem Cells and Gene Regulation, National Institute of Arthritis and Musculoskeletal and Skin Disease, Bethesda, MD 20892, USA.
*These authors contributed equally to this work

‡Authors for correspondence (utz.fischer@biozentrum.uni-wuerzburg.de; matthias.becker@uni-wuerzburg.de)

M.H., 0000-0002-4336-6518; U.F., 0000-0002-1465-6591

Handling Editor: Giampietro Schiavo
Received 19 November 2020; Accepted 11 May 2021

Journal of Cell Science (2021) 134, jcs257535. doi:10.1242/jcs.257535

results in the loss of neural mRNA signatures. Intriguingly, the direct miR-26-mediated inhibition of REST and CTDSPs enables the expression of REST-regulated miRs and, as a consequence, sets in train the gene expression program required for the differentiation of NPCs into NCs. Our data identify the miR-26 family as an upstream trigger for a self-amplifying neuronal miR network that induces the differentiation of NPCs into NCs.

RESULTS

Arrest of NPC differentiation upon deletion of miR-26 family members

To analyze the role of miR-26 family members in neurogenesis, we used a murine ESC-based neural differentiation system that allows *ex vivo* differentiation of murine ESCs into NPCs within 9 days. Within an additional 6 days, the differentiation of NPCs into NCs, including postmitotic neurons and, to a lesser extent, glial cells, is completed (for a schematic representation of the differentiation protocol, see Fig. S1A). Neurogenesis is faithfully recapitulated in this system, based on cell morphology criteria as well as expression profiles of established cellular and molecular markers (Abranches et al., 2009; Bibel et al., 2007a,b; Dinger et al., 2008; Wolber et al., 2013).

First, the expression levels of mature miR-26a and miR-26b were analyzed (Fig. 1A). During differentiation of ESCs into NCs (day 15), miR-26a and miR-26b levels increased ∼7-fold, which is consistent with their proposed role in neurogenesis. Of note, expression of mature miR-26a in ESCs and NCs was about 3-fold higher than miR-26b expression (Fig. 1B). In contrast, the transcript levels of precursor miR-26 peaked early in differentiation (day 3) and declined from thereon to reach levels at the NC stage below those measured in ESCs (Fig. S1B). The transcript levels of the Ctdsp host genes peaked at day 9 of differentiation (Fig. S1B). To analyze the expression of precursor miR-26, mature miR-26 and the Ctdsp host genes *in vivo*, we monitored their transcript levels during mouse brain development. We found that, in analogy to our *in vitro* model, expression of pre-miR-26 and the Ctdsp genes peaked earlier in development than the expression of mature miR-26 (Fig. S1C). Taken together, these data show that Ctdsp and miR-26 expression, as well as miR-26 maturation, are developmentally regulated.

To evaluate the function of the miR-26 family during neural differentiation, we applied the CRISPR/Cas9 system to generate a KO of miR-26b (KO^{26b}), a double KO (dKO) of miR-26a1 and miR-26a2 ($dKO^{26a1/a2}$) and a triple KO (tKO) of all three family members ($tKO^{26b/a1/a2}$) in ESCs (see Fig. S2A–D for a comprehensive characterization of KO cell lines).

Several lines of evidence indicate that the initial differentiation step from ESCs to NPCs proceeds normally in cells lacking miR-26. First, all miR-26 KO cell lines formed colonies of normal ESC-type morphology and appearance (Fig. S3A). Second, wild-type (WT) and KO ESCs expressed similar transcript levels of the core pluripotency genes *Oct4*, *Sox2*, *Nanog* and *Rex1* (also known as *Zfp42*) (Fig. S3B). Third, cumulative population doublings of ESCs, as well as cell numbers under embryoid body (EB) differentiation conditions, were similar in WT and KO cultures (Fig. S3A,C,D). Lastly, equal frequencies of cells expressing the NPC markers SOX2, nestin (Fig. S3A,E) and musashi1 (MSI1) (Fig. S3F) were observed in WT and KO cultures when cultivated under conditions that generated a defined population of NPCs from ESCs. Thus, the deletion of individual miR-26 family members or deletion of the entire miR-26 family affects neither ESC identity nor their differentiation into NPCs.

We next assessed whether miR-26 KO affects the differentiation from NPCs into NCs. WT NPCs differentiated into cells with characteristic neuronal morphologies. These cells also displayed expression of the neuronal markers TUBB3 and MAP2 as well as the astroglia marker GFAP, indicating formation of NCs (Fig. 1C). In contrast, the majority of cells lacking miR-26 members failed to acquire neuronal morphologies, and only a small fraction of cells expressed TUBB3, MAP2 or GFAP. Of note, KO of miR-26b alone or dKO of miR-26a1 and miR-26a2 was sufficient to interfere with NC differentiation, albeit to different degrees (Fig. 1C). Thus, the lack of one miR-26 variant cannot be compensated by remaining family members. Taken together, these data indicate that all miR-26 family members are critical for the generation of neurons and astrocytes from NPCs.

We next assessed whether miR-26 KO cultures are stalled in differentiation. Immunostaining of day 15 cultures revealed that the frequencies of $SOX2^+$, $nestin^+$ and $MSI1^+$ cells increased in miR-26-deficient cultures (Fig. 1D), indicating an increased number of neural progenitor and/or stem cells. In parallel, the frequencies of cells positive for apoptotic markers [i.e. annexin 5 (ANXA5) and propidium iodide (PI)] remained unaltered in miR-26 KO cultures (Fig. S4A). Thus, the lack of differentiated NCs in miR-26-deficient cultures was not due to their selective elimination during differentiation but rather indicates that the cells were arrested at the NPC level. Analysis of cell cycle phase distributions indicate increased frequencies of cells in S, M, and G_2 phases and fewer cells in the G_1 phase in day 15 $tKO^{26b/a1/a2}$ NC cultures (Fig. S4B). In addition, the expression of cell cycle inhibitors $p16^{Ink4A}$, $p19^{Arf}$ (both encoded by *Cdkn2a*) and $p21^{Cip1}$ (encoded by *Cdkn1a*) was reduced in miR-26 KO NCs, linking the miR-26 family to cell cycle regulation (Fig. S4C). To ask whether the cycling population in $tKO^{26b/a1/a2}$ cultures indeed consists of NPCs, we next determined the frequencies of $BrdU^+$ cells as well as the $BrdU^+$:$Msi1^+$ cell ratio at day 10 and day 12 of differentiation in $tKO^{26b/a1/a2}$ and WT cultures (Fig. S4D). Consistent with an increased frequency of NPCs, these analyses revealed that $MSI1^+$ cell frequencies were also increased at day 12 of differentiation in $tKO^{26b/a1/a2}$ cultures. At this time point, frequencies of $BrdU^+$ cells were also increased in $tKO^{26b/a1/a2}$ cultures. Our analyses further showed that the ratio of $BrdU^+$:$MSI1^+$ cells was at the same level in WT and $tKO^{26b/a1/a2}$ cultures, indicating that most of the cells in cycle in WT and $tKO^{26b/a1/a2}$ cultures were indeed NPCs. Taken together, the analyses of miR-26 KO cultures revealed that differentiation of ESCs to NPCs remained unaffected, whereas NPC differentiation into NCs was arrested in KO cultures.

To eliminate potential secondary effects caused by the generation of KO cell lines, miR-26-deficient $tKO^{26b/a1/a2}$ NPCs were transiently transfected with a mixture of synthetic miR-26a and miR-26b mimics. Frequencies of $TUBB3^+$ neuronal cells, as well as frequencies of $SOX2^+$ and $nestin^+$ NPCs, were then compared to those in WT cultures at day 15 of differentiation. As shown in Fig. 2, synthetic miR-26a and miR-26b almost completely rescued the neuronal differentiation block in $tKO^{26b/a1/a2}$ cells, as evidenced by the increase of $TUBB3^+$ NC cell frequencies and the reduced frequencies of $SOX2^+$ and $nestin^+$ NPCs. Thus, the observed developmental block in NPC differentiation is a direct consequence of miR-26 loss.

miR-26 KO results in downregulation of neural transcription programs

We next conducted experiments designed to illuminate at the molecular level how miR-26 evokes its effects on neural

Journal of Cell Science (2021) 134, jcs257535. doi:10.1242/jcs.257535

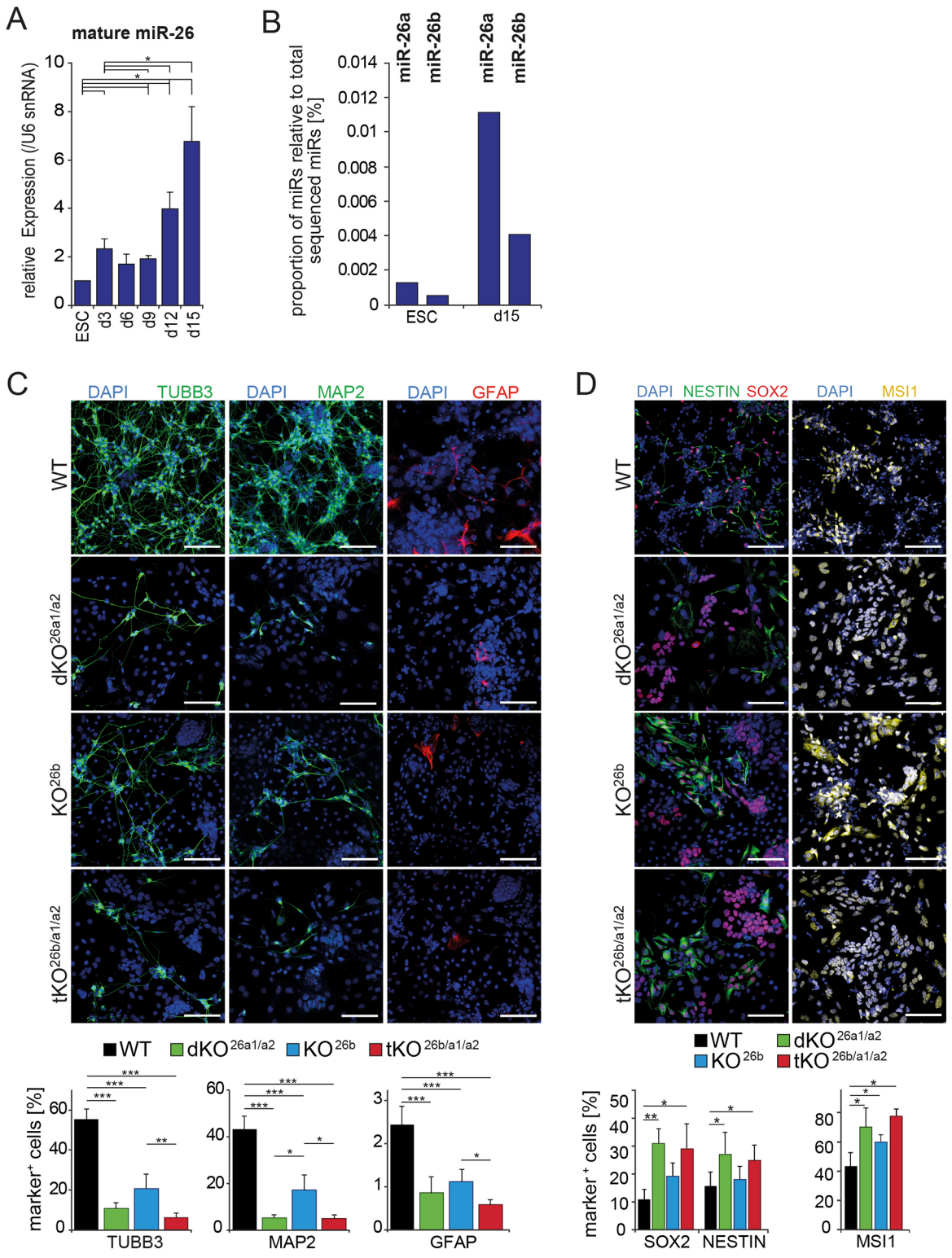

Fig. 1. Differentiation of miR-26 KO NPC cultures leads to reduced frequencies of neurons and astrocytes and increased frequencies of neural progenitors. (A) RT-qPCR analysis of mature miR-26 expression during wild-type (WT) differentiation (d, day of differentiation). *n*=4 biological replicates, mean±s.d. **P*<0.05 (paired, two-tailed *t*-test). (B) Mature miR-26a and miR-26b expression levels as a percentage of total miR expression level, as determined by RNA-seq. (C) Representative immunostaining of neuronal and glial markers in the indicated cell cultures after 15 days of differentiation. Percentage of cells positive for neuronal (TUBB3, MAP2) and astroglial (GFAP) markers are shown beneath. *n*=4 biological replicates, mean±s.d. (D) Representative immunostaining of neural progenitor markers in the indicated cell cultures at 15 days of differentiation. Percentage of cells positive for the neural progenitor (SOX2, nestin and MSI1) markers are shown beneath. *n*=4 biological replicates, mean±s.d. Nuclei are stained using DAPI. Scale bars: 100 µm. **P*<0.05, ***P*<0.01, ****P*<0.001 (one-way ANOVA with Tukey's post hoc test).

Journal of Cell Science (2021) 134, jcs257535. doi:10.1242/jcs.257535

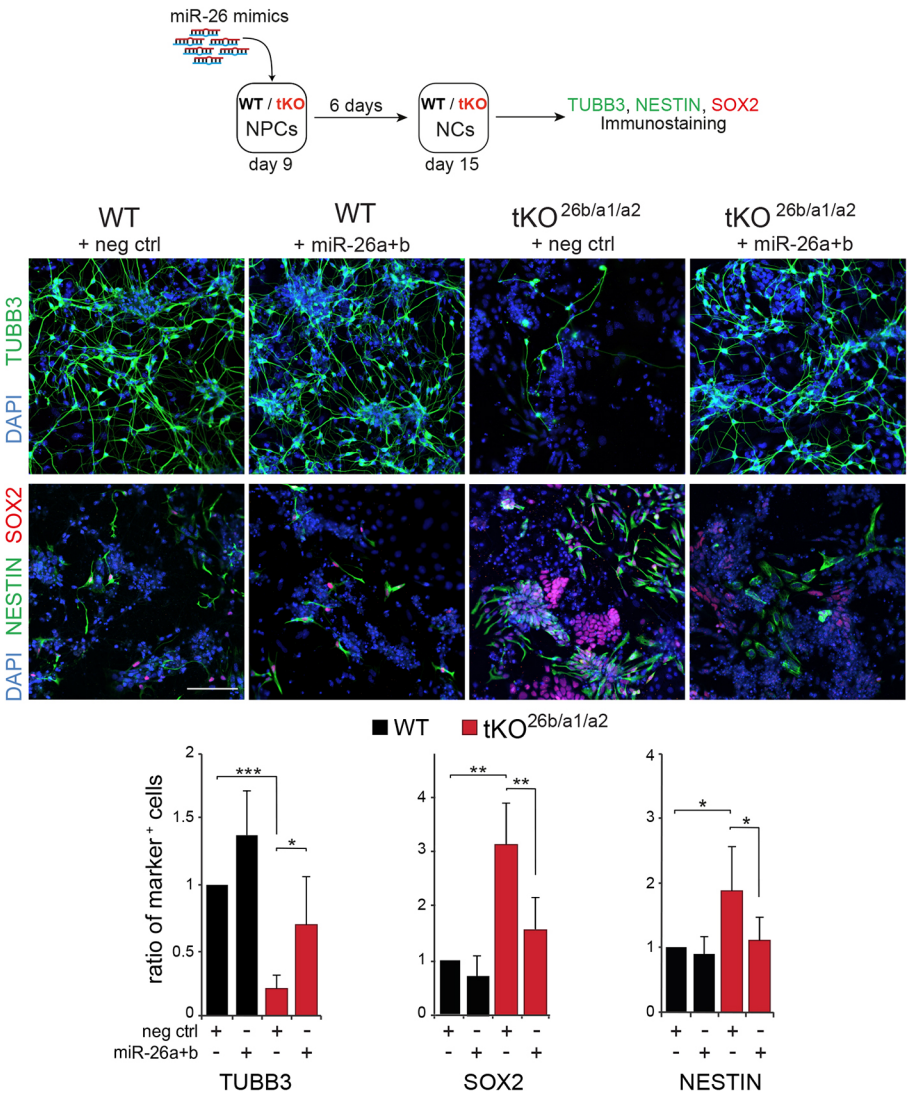

Fig. 2. Rescue of the miR-26 KO phenotype upon reintroduction of miR-26 mimics. Top: schematic representation of the experimental strategy (upper panel). Middle: representative immunostainings of WT and tKO$^{26b/a1/a2}$ cultures transfected with either negative control (neg ctrl) or miR-26a and miR-26b mimics (miR-26a+b) stained for neural progenitor markers (nestin, SOX2) and the marker for postmitotic neurons TUBB3. Nuclei are stained using DAPI. Bottom: quantification of marker-positive cells for the different markers. n=4 biological replicates, mean ±s.d. Scale bar: 100 µm. *P<0.05, **P<0.01, ***P<0.001 (one-way ANOVA with Tukey's post hoc test).

differentiation. We performed global gene expression profiling of WT and tKO$^{26b/a1/a2}$ cultures differentiated for 15 days. Transcripts with an expression level that differed by at least a factor of 4 between WT and tKO$^{26b/a1/a2}$ were considered significantly affected and, hence, were analyzed further. Of the transcripts that met this criterion, 943 were increased in tKO$^{26b/a1/a2}$ cultures compared with their levels in WT cultures, whereas 543 were decreased (Fig. 3A). Characterisation of the increased transcripts using gene ontology (GO) term enrichment algorithms showed no obvious tendency for a particular biological process (Fig. 3B). In contrast, GO term analysis of transcripts with reduced expression in tKO$^{26b/a1/a2}$ cultures revealed that 14 of the 40 top enriched terms have a neural affiliation (see GO terms highlighted in red in Fig. 3C). Thus, ablation of miR-26 negatively affects the expression of neuronal genes, which is consistent with the observed defect in differentiation (see Fig. 1).

The RNA-seq analysis described above was performed to determine transcript levels at the endpoint of NC differentiation. Next, we investigated by RT-qPCR the expression of selected neuronal markers that were identified as being differentially expressed in our global gene expression analyses during differentiation of ESCs into NCs. As expected, expression of the neuronal markers *Tubb3*, *Neurod1*, *Neurog1* and *Ncam1* gradually increased in WT cultures, starting with low levels in ESCs and displaying their highest levels at the NC stage (day 15). In contrast, although the expression of these markers in tKO$^{26b/a1/a2}$ cultures also increased in the initial phase (i.e. up to NPC stage, day 10), their transcript levels remained largely constant thereafter (*Tubb3*, *Neurog1* and *Ncam1*) or only slightly increased (*Neurod1*) (Fig. 3D). The NPC markers *Msi1* and *Pax6* increased in WT and tKO$^{26b/a1/a2}$ cultures during differentiation from ESC to NPC, confirming that both cell lines can develop into NPCs. However, a decrease in expression of these markers as a hallmark of NC formation was observed only in WT cultures, whereas the levels remained unaltered in the tKO$^{26b/a1/a2}$ cells (Fig. 3D). Thus, the transcriptional program promoting the differentiation of ESCs into NPCs is still active in the absence of miR-26; however, the subsequent establishment of the gene expression program required for the formation of neurons and astrocytes from NPCs is severely affected.

Inactivation of miR-26 affects the expression of *Rest* and *Ctdsp2*

We next asked how miR-26 exerts its specific impact on neural gene expression. miR-26b has been linked to the regulation of Ctdsp2 in zebrafish (Dill et al., 2012), and proteins encoded by the miR-26

Journal of Cell Science (2021) 134, jcs257535. doi:10.1242/jcs.257535

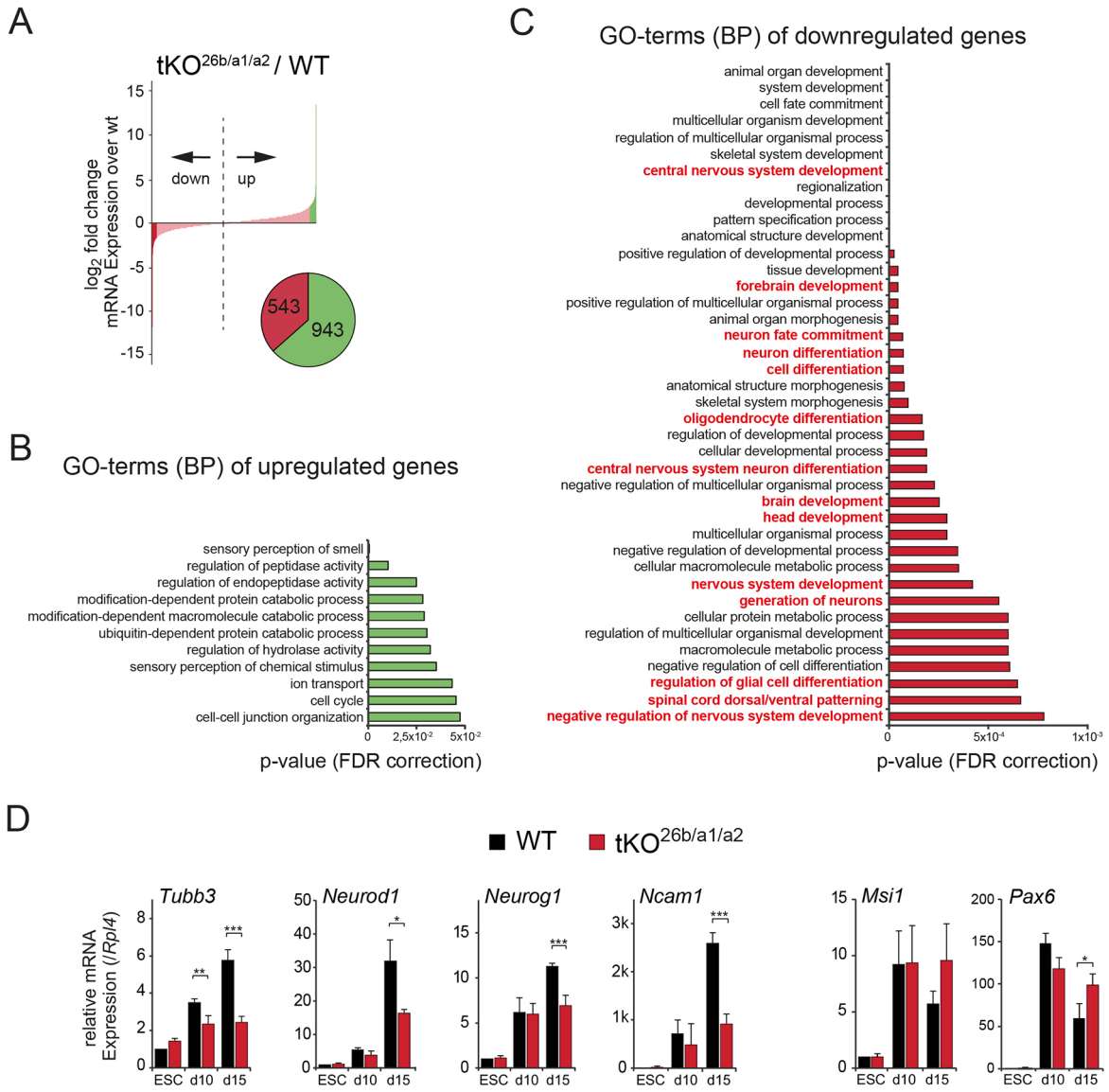

Fig. 3. Neuronal transcripts are globally reduced in differentiated miR-26 KO NC cultures. (A) Global downregulated and upregulated genes in tKO$^{26b/a1/a2}$ cultures compared to WT NC cultures. Bar graph shows ranked $\log_2$ fold change in mRNA expression. Pie chart indicates numbers of downregulated (red) and upregulated (green) transcripts (threshold >4-fold). (B) GO term analysis of upregulated transcripts. All biological process (BP) GO terms that were retrieved in the analysis are shown, with significance of their enrichment among the upregulated transcripts indicated. FDR, false discovery rate. (C) GO term analysis of downregulated transcripts. The top 40 most significantly enriched BP GO terms are shown. GO terms associated with neural development are marked in red. (D) RT-qPCR analysis of neuronal markers (*Tubb3*, *Neurod1*, *Neurog1* and *Ncam1*) and neural progenitor markers (*Msi1*, *Pax6*) using WT or tKO$^{26b/a1/a2}$ ESCs, NPCs (d10) and NCs (d15). n=3 biological replicates, mean±s.d. *P<0.05, **P<0.01, ***P<0.001 (one-way ANOVA with Tukey's post hoc test).

Ctdsp host genes are part of the REST complex (Yeo et al., 2005), which is a major regulator of neuronal gene expression. We therefore speculated that miR-26 affects mammalian neuronal gene expression via the REST complex. Furthermore, bioinformatic analyses using TargetScan 7.1 (Agarwal et al., 2015) of REST complex components revealed that, in addition to *Ctdsp2*, the *Rest* and *CoRest* mRNAs also contain at least one predicted miR-26 target site in their 3′ untranslated region (UTR). We thus examined how inactivation of miR-26 affects expression of REST and its cofactors during neuronal differentiation. SIN3A, a component of the REST complex lacking a predicted miR-26 target site, was included as control. WT and tKO$^{26b/a1/a2}$ cultures were differentiated as described above, and protein levels of REST and its cofactors were determined using western blotting. CoREST and SIN3A did not show differential expression in tKO$^{26b/a1/a2}$ cultures in comparison to WT cultures during differentiation (Fig. 4A,B). In contrast, REST and CTDSP2 protein levels in tKO$^{26b/a1/a2}$ cultures were only comparable to the levels observed in WT cultures in the initial differentiation phase (up to day 8). This changed, however, in later phases of differentiation, where protein levels of CTDSP2 and REST were significantly increased as compared to the levels in WT cultures (compare black and red bars in Fig. 4B). Thus, loss of miR-26 prevents downregulation of REST and CTDSP2 at the NPC stage and at later stages, providing an explanation for the observed lack of neuronal gene expression programs in miR-26-deficient cultures.

Comparison of mRNA expression levels of all Ctdsp homologs in differentiating WT and tKO$^{26b/a1/a2}$ cultures (Fig. 4C) showed that, whereas Ctdsp mRNA expression declined in WT cultures during

Journal of Cell Science (2021) 134, jcs257535. doi:10.1242/jcs.257535

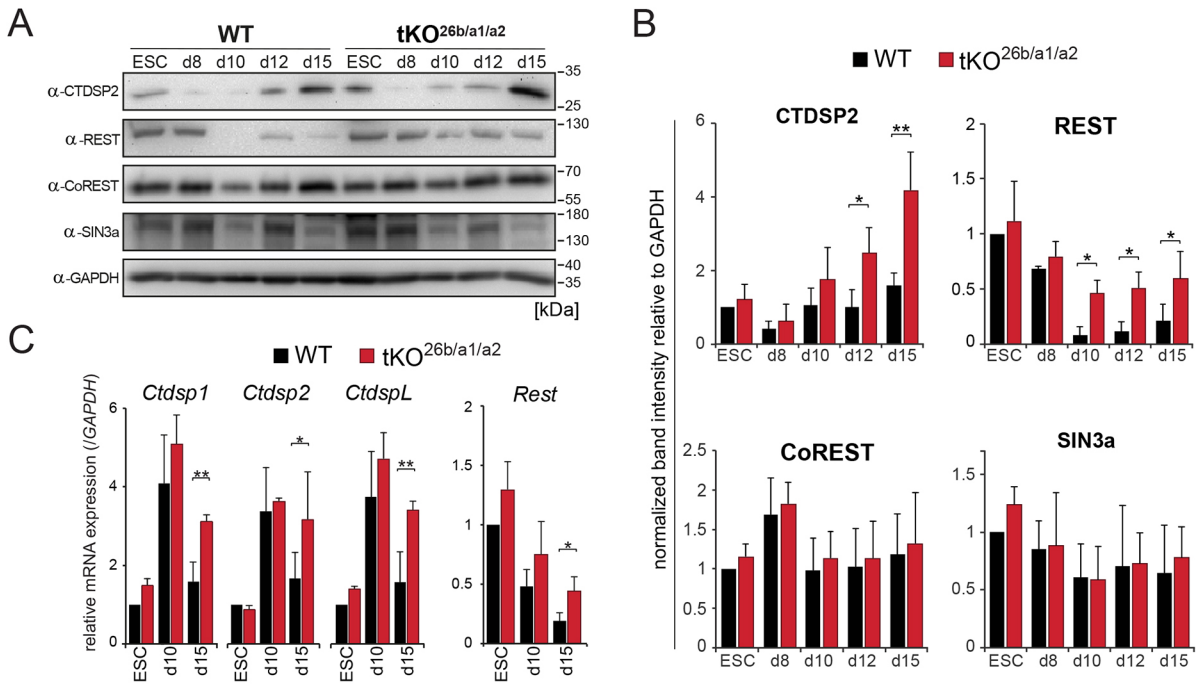

Fig. 4. miR-26 affects expression of REST complex members at the RNA and protein level. (A) Representative western blots of REST complex components (REST, CoREST, CTDSP2, SIN3A) and GAPDH as loading control in WT and tKO$^{26b/a1/a2}$ cell cultures at different time points during differentiation (d, days of differentiation). (B) Quantification of western blot band intensities relative to GAPDH protein levels, *n*=3 biological replicates, mean ±s.d. **P*<0.05, ***P*<0.01 (one-way ANOVA with Tukey's post hoc test). (C) RT-qPCR analysis of *Ctdsp1*, *Ctdsp2*, *CtdspL* and *Rest* expression in WT and tKO$^{26b/a1/a2}$ ESCs, NPCs (d10) and NCs (d15). *n*=4 biological replicates, mean±s.d. **P*<0.05, ***P*<0.01 (one-way ANOVA with Tukey's post hoc test).

differentiation from NPCs to NCs, Ctdsp expression remained constant in tKO$^{26b/a1/a2}$ cultures. As only *Ctdsp2* is a potential direct target for miR-26, the effect on *Ctdsp1* and *CtdspL* mRNA levels is likely to be caused indirectly. *Rest* mRNA expression in WT cells was highest in ESCs and declined during differentiation to NCs. Similar to Ctdsp mRNAs, we also observed higher *Rest* mRNA expression levels in tKO$^{26b/a1/a2}$ NC cultures compared to levels in WT NC cultures. In conclusion, these data show that expression of Ctdsp mRNA and *Rest* is regulated by miR-26 during NPC to NC differentiation.

miR-26 directly targets *Rest* and *Ctdsp2*

Next, we tested whether the miR-26 family directly targets *Rest* and *Ctdsp2* mRNA, which was likely as we identified putative miR-26 target sites in the 3′ UTR of both mRNAs. To analyze this possibility, we fused the 3′ UTRs encoding the WT miR-26 target sites of *Ctdsp2* and *Rest* each to a luciferase reporter and measured reporter expression (see schematic representation in Fig. 5A). As controls, we tested identical constructs that only differed from the WT constructs in harboring mutated miR-26 binding sites. Bioinformatic analyses revealed one potential miR-26 target site at position 2971–2977 of the *Ctdsp2* 3′ UTR and two potential miR-26 target sites in the 3′ UTR of *Rest* at positions 346–353 (8mer target site) and 2519–2525 (7mer target site), respectively. Upon co-transfection with miR-26a or miR-26b mimics into HEK 293T cells, both *Ctdsp2* and *Rest* WT reporter constructs yielded reduced luciferase activity in comparison to activity in cells co-transfected with a negative control miR mimic (Fig. 5A). In contrast, the reporter constructs harboring the mutated miR-26 binding site in the *Ctdsp2* 3′ UTR or the mutated 8mer binding site in the *Rest* 3′ UTR showed no significant change in luciferase activity, indicating that these binding sites are direct miR-26 targets. A reporter construct harboring the mutated 7mer target site in the *Rest* 3′ UTR yielded the same reduction in luciferase activity as the WT *Rest* 3′ UTR, indicating that this site is not targeted by miR-26. These data show that only the 8mer site is a functionally active miR-26 target in the *Rest* 3′ UTR.

We next asked whether miR-26 directly targets endogenous *Ctdsp2* and *Rest*. To this end, we generated ESC cultures with CRISPR/Cas9-directed deletion of the miR-26 target sites (ts) in the 3′ UTRs of *Ctdsp2* and *Rest*. As depicted in the schematic representation (Fig. 5B), the deleted sequence in *Ctdsp2* spanned 30 nucleotides. Due to the unfavorable location of protospacer adjacent motif (PAM) sequences we introduced a larger, 250-nucleotide-spanning deletion centered on the miR-26 ts in the *Rest* 3′UTR (Fig. 5B). RNA expression analyses revealed that, compared to levels in WT cells, *Ctdsp2* mRNA levels were increased at day 15 of differentiation in the *Ctdsp2* miR-26 ts KO cells (Fig. 5C), suggesting that endogenous *Ctdsp2* is indeed a target of miR-26 during neural differentiation. The expression of *Ctdsp1*, *CtdspL* and *Rest* were unaffected in the *Ctdsp2* miR-26 ts KO cells. In *Rest* miR-26 ts KO cells, *Rest* mRNA levels were increased at day 10 and day 15 of differentiation compared to levels in WT cells (Fig. 5D). Interestingly, deletion of the *Rest* miR-26 ts did not only affect *Rest* expression but also affected the expression of *Ctdsp2* and *CtdspL* at day 15 of differentiation. Taken together, these results are consistent with both endogenous *Ctdsp2* and *Rest* being miR-26 targets during neural differentiation. We moved on to ask whether the miR-26 ts deletions in endogenous *Ctdsp2* or *Rest* had an effect on neuronal differentiation. Immunofluorescence analyses revealed that in day 15 *Ctdsp2* miR26 ts KO cultures the number of neurons (as determined by the proportion of TUBB3^{+} cells) was similar to those observed in WT controls, whereas *Rest* miR-26 ts KO resulted in reduced number of neurons (Fig. 5E, upper graph). The

Journal of Cell Science (2021) 134, jcs257535. doi:10.1242/jcs.257535

reduced number of neurons was, however, not as pronounced as in tKO$^{26b/a1/a2}$ cultures. We also determined the frequencies of nestin^{+} and SOX2^{+} cells (Fig. 5E, lower graph) and found that, in comparison to WT cultures, *Rest* miR-26 ts KO cultures showed increased frequencies of nestin^{+} and SOX2^{+} cells. The number of cells positive for these NPC markers in *Rest* miR-26 ts KO cultures

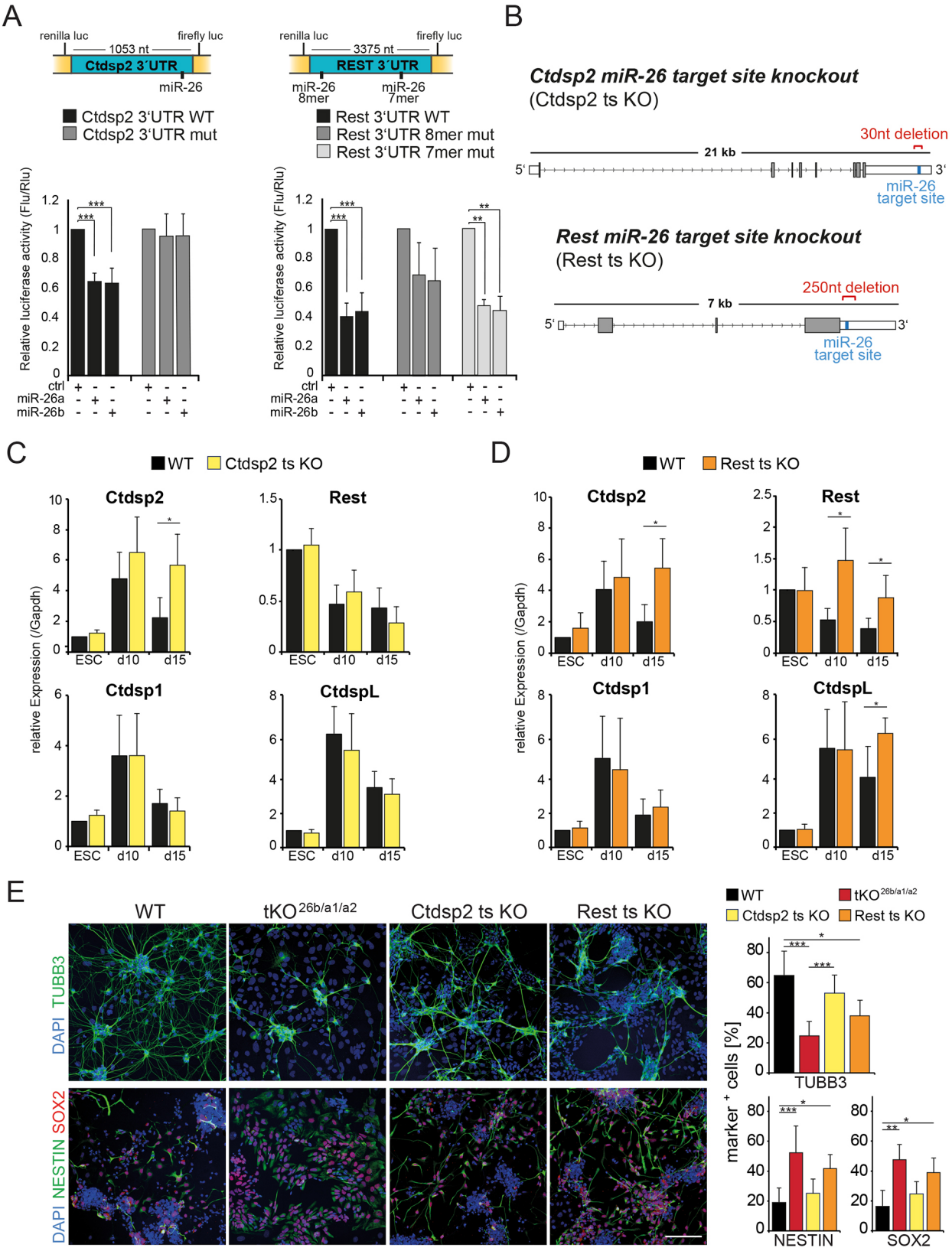

Fig. 5. See next page for legend.

Journal of Cell Science (2021) 134, jcs257535. doi:10.1242/jcs.257535

Fig. 5. miR-26 directly targets *Rest* and *Ctdsp2* expression. (A) Schematic representation of *Rest* and *Ctdsp2* 3′ UTR luciferase (luc) reporter constructs (upper panel; nt, nucleotides). Dual-luciferase assays with WT and miR target site mutated (mut) *Rest* and *Ctdsp2* 3′ UTR reporter constructs (lower panel). Reporter constructs were co-transfected together with either control (ctrl)-, miR-26a- or miR-26b-mimics into HEK293T cells. Relative luciferase activities were determined 24 h post transfection (Flu, firefly luciferase; Rlu, *Renilla* luciferase). *n*=5 biological replicates, mean±s.d. ***P*<0.01, ****P*<0.001 (one-way ANOVA with Tukey's post hoc test). (B) Schematic representation of *Ctdsp2* and *Rest* target site deletion (ts KO) in the genomic context. The position of miR-26 target sites and size of deletion are indicated. (C,D) *Ctdsp1*-, *Ctdsp2*-, *CtdspL*- and *Rest*-specific RT-qPCR analyses of (C) WT and *Ctdsp2* ts KO, and (D) WT and *Rest* ts KO cells at day 0 (ESC), day 10 (d10) and day 15 (d15) of differentiation. *n*=5 biological replicates, mean±s.d. **P*<0.05 (one-way ANOVA with Tukey's post hoc test). (E) Representative immunostainings of WT, $tKO^{26b/a1/a2}$, *Ctdsp2* ts KO and *REST* ts KO cell cultures (day 15 of differentiation, left), stained for the indicated markers and with nuclei labeled using DAPI. Percentage of $TUBB3^+$, $nestin^+$ and $SOX2^+$ cells are shown on the right. *n*=3 biological replicates, mean±s.d. Scale bar: 100 µm. **P*<0.05, ***P*<0.01, ****P*<0.001 (one-way ANOVA with Tukey's post hoc test).

was almost as high as the number observed in $tKO^{26b/a1/a2}$ cultures. In contrast, the frequency of NPC marker-positive cells observed in *Ctdsp2* miR-26 ts KO cultures was similar to that in WT cultures. Taken together, these analyses show that the *Rest* miR-26 ts KO led to reduced neuronal differentiation and increased frequencies of NPCs. Thus, the *Rest* miR-26 ts KO largely mimicked the $tKO^{26b/a1/a2}$ phenotype, whereas the miR-26 ts KO in *Ctdsp2* had no effect on neuronal differentiation.

miR-26 unleashes transcriptional repression of a neuronal miR network

Upon targeting the REST complex during differentiation, miR-26 may also affect the expression of many other miRs. Hence, we first analyzed by systematic miR sequencing (miR-seq) how KO of miR-26 affected expression of other miRs. We found that 628 miRs were differentially expressed in $tKO^{26b/a1/a2}$ cultures when compared to expression in WT cultures, the majority (66%) being upregulated (Fig. 6A). When focusing on miRs that are putatively regulated by REST due to the presence of an RE1 site in their promoter region (REST-miRs) (Conaco et al., 2006; Johnson and Buckley, 2009), we noted that all but one were downregulated in $tKO^{26b/a1/a2}$ cultures (Fig. 6A). Analyses of two of the identified REST-miRs (miR-124 and miR-9) in $tKO^{26b/a1/a2}$ and WT cultures during differentiation confirmed that expression of these miRs was reduced in $tKO^{26b/a1/a2}$ NC cultures (day 15) (Fig. 6B). We also found that both miR-9 and miR-124 were downregulated in differentiating *Rest* miR26 ts KO cells (Fig. 6C), further supporting the notion that miR-26 exerts its function mainly through targeting *Rest*. Moreover, all of the downregulated REST-miRs have at least two predicted target sites in mRNAs encoding REST complex components, and hence have the potential to feedback on their own transcription (Fig. S6A).

The expression of the miR-26 family is controlled by as yet unknown regulators that may control DICER processing. This family therefore likely differs from other neuronal miRs that are under transcriptional control. This predisposes the miR-26 family members to a role upstream of other miRs acting in neurogenesis and would imply that miR-26 can activate REST-miRs, but not vice versa. To test this notion, we transfected miR-26 mimics into WT and $tKO^{26b/a1/a2}$ NPC cultures and measured REST-miR expression levels 3 days later using RT-qPCR. As shown in Fig. 6D, this led to elevated levels of REST-miRs (miRs-9, -124, -218 and -135a) in WT cultures. Furthermore, while REST-miR levels were reduced in $tKO^{26b/a1/a2}$ cultures, the transfection of miR-26 mimics rescued this effect. This observation shows that miR-26 family members influence the expression of REST-miRs, most likely via regulation of the REST–CTDSP pathway.

Finally, we tested whether miR-26 acts upstream of REST-miRs. In this case, REST-miRs such as miR-9 and miR-124 should have no impact on the expression levels of miR-26. To test this, miR-9 and miR-124 mimics were transfected into WT NPC cultures, and miR expression levels were determined (Fig. 6E). In contrast to miR-26, which was sufficient to increase REST-miR levels (Fig. 6A), miR-9 and miR-124 failed to influence miR-26 levels (Fig. 6E). Transfection of these miRs, however, increased levels of REST-miRs such as miR-9, miR-124, miR-218 and miR-135a. These findings indicate that miR-26 family members act as early regulators of neurogenesis, controlling neural miRs (REST-miRs) and RE1-containing genes (Fig. S6B,C) by affecting REST complex activity (see Fig. 6F for a schematic model).

DISCUSSION

A role of miR-26b in neurogenesis was first established in zebrafish (Dill et al., 2012), but the function of this miR in mammals and its mode of action in the regulation of neuronal gene expression has remained unclear. Here, we report on a critical role of the mammalian miR-26 family in neurogenesis, specifically in the differentiation of NPCs to neurons and astrocytes. This function is mirrored by miR-26 expression profiles; expression and conversion into the mature forms occur only after the NPC stage and, consequently, miR-26 deletion only affects post-NPC differentiation stages. Consistent with this, deletion of the miR-26 target sites in *Ctdsp2* and *Rest* only affected their expression at the NPC and NC stages.

miR-26 KO cells were more frequently arrested at the NPC stage than WT cells. KO cells were not apoptotic but remained in the cell cycle. This is in agreement with the reduced expression of cell cycle inhibitors $p16^{Ink4A}$, $p19^{Arf}$ and $p21^{Cip1}$ in KO cells. BrdU labeling of WT and $tKO^{26b/a1/a2}$ cells indicated that most of the BrdU-positive cells in both cultures were indeed NPCs. Published data show that neuronal differentiation of adult NSCs can be promoted by cell cycle inhibition (Roccio et al., 2013). It is therefore tempting to speculate that differentiation of miR-26 KO cells is impaired due an incapability to exit the cell cycle. The effects on cell cycle progression are in agreement with previous observations that ectopic miR-26a expression suppresses cell proliferation by inducing a G_1 phase arrest (Lu et al., 2011). Likewise, a G_1-S transition block has been reported following overexpression of miR-26a or -26b (Zhu et al., 2012). During neurogenesis, a reduction of G_1-phase length results in inhibition, whereas an extension of G_1 phase promotes differentiation (Artegiani et al., 2011; Lange et al., 2009; Lim and Kaldis, 2012). Future work should therefore address the question of whether miR-26 KO results in a reduced G_1-phase duration. We noted that the phenotype of $dKO^{26a1/a2}$ on neurogenesis was more drastic than that of miR-26b KO. This might be due to the 3-fold higher expression level of miR-26a1/2 over miR-26b. Rather unexpectedly, however, KO of either miR-26b or miR-26a1/a2 alone affected neuronal differentiation, despite the remaining miR-26 family members being present. The lack of compensation is surprising, as the mature sequences of miR-26b and miR-26a1/a2 differ in only two nucleotides, and their seed sequences are identical. This could indicate a dosage effect, since transfection with miR-26a or miR-26b mimics rescues the differentiation of $tKO^{26b/a1/a2}$ NCs with similar efficiencies.

Journal of Cell Science (2021) 134, jcs257535. doi:10.1242/jcs.257535

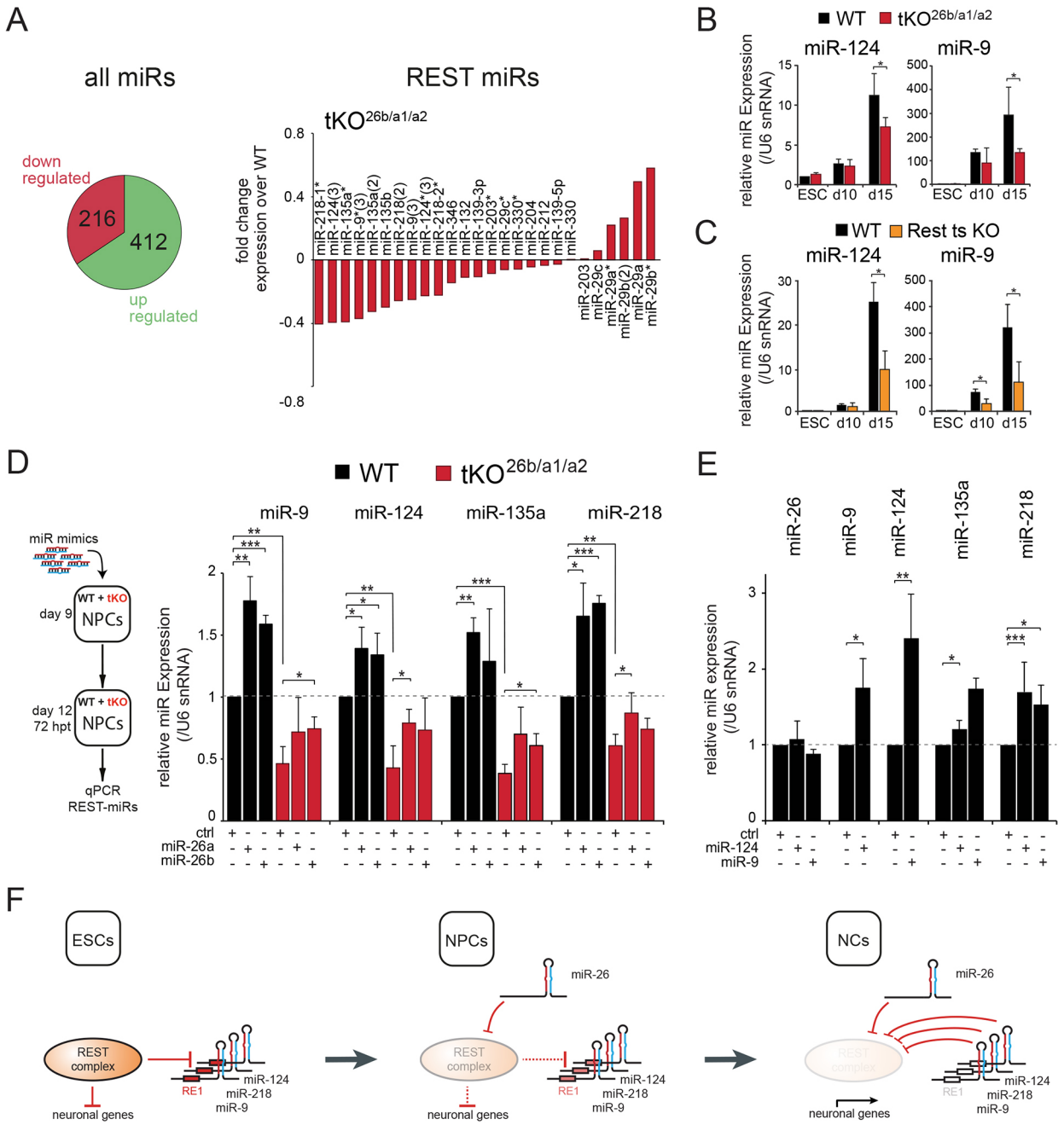

Fig. 6. The miR-26 family acts upstream of REST-regulated miRs. (A) Global downregulated and upregulated miRs in tKO$^{26b/a1/a2}$ cells compared to WT cells at day 15 of differentiation. Pie chart (left) shows numbers of downregulated and upregulated miRs. Graph (right) shows fold change in expression levels of REST-regulated miRs in tKO$^{26b/a1/a2}$ cultures compared to levels in WT cultures. (B,C) RT-qPCR analysis of miR-124 and miR-9 in WT, tKO$^{26b/a1/a2}$ (B) and *Rest* ts KO (C) cells at day 0 (ESC), day 10 (d10) and day 15 (d15) of differentiation. n=3 biological replicates, mean±s.d. *P<0.05 (one-way ANOVA with Tukey's post hoc test). (D) RT-qPCR analyses probing the expression of REST-regulated miRs in WT and tKO$^{26b/a1/a2}$ cell cultures 72 h after transfection (hpt) with miR-26a, miR-26b or control (ctrl) miR mimics at day 9 of differentiation. n=4 biological replicates, mean±s.d. *P<0.05, **P<0.01, ***P<0.001 (one-way ANOVA with Tukey's post hoc test). (E) miR-26-, miR-9-, miR-124-, miR-218- and miR-135a-specific RT-qPCR analyses of WT cell cultures 72 h after transfection with miR-124, miR-9 or control miR mimics at day 9 of differentiation. n=4 biological replicates, mean±s.d. *P<0.05, **P<0.01, ***P<0.001 (one-way ANOVA with Tukey's post hoc test). (F) Model of the REST complex/miR-26 negative feedback cascade during neuronal differentiation. In undifferentiated ESCs, the REST complex inhibits expression of neuronal genes and miRs via binding to RE1 sequences. In NPCs, miR-26 family members are processed and inhibit expression of their Ctdsp host genes as well as the REST core component. In consequence, neuronal miRs become expressed and target mRNAs of further REST complex components.

REST suppresses neuronal gene expression and regulates the transition from pluripotent ESCs to NPCs and from NPCs to mature neurons (Ballas et al., 2005). We observed that miR-26 KO affected neither the undifferentiated ESCs, nor the differentiation of ESC to NPCs. This is in agreement with the minor effects of tKO$^{26b/a1/a2}$ on REST and CTDSP protein levels up to the NPC stage. However, we observed elevated REST and CTDSP mRNA and protein levels in tKO$^{26b/a1/a2}$ cultures compared to levels in WT NC cultures. The arrest of later differentiation stages in tKO$^{26b/a1/a2}$ cultures indicate stage-specific functions of the miR-26 family, either in the context

Journal of Cell Science (2021) 134, jcs257535. doi:10.1242/jcs.257535

of the REST complex and/or REST independently. In this regard, our data shows that miR-26 targets *Rest* and *Ctdsp2* directly. Deletion of the miR-26 target site in the REST complex cofactor *Ctdsp2* only affected the expression of *Ctdsp2*, but affected neither the expression of *Rest* and other *Ctdsp* family members nor neural differentiation. This is in contrast to earlier studies in zebrafish that have shown a rescue of the miR-26-knockdown-mediated reduction of neurons when Ctdsp2 is reduced simultaneously (Dill et al., 2012), suggesting species-specific differences in the function of CTDSP2. In contrast, the deletion of the *Rest* miR-26 ts almost completely phenocopied the $tKO^{26b/a1/a2}$ situation and also affected *Ctdsp2* and *CtdspL* mRNA expression. This is consistent with a key role for REST in the miR-26-mediated regulation of neuronal gene expression and suggests a regulation of the REST complex at the network level rather than on the level of individual genes. Our own bioinformatic analyses further revealed that the miR-26 target sites in the *Rest* 3′ UTR are conserved in human and mouse, but not in zebrafish. This notion is in agreement with previously published data on miR-125-mediated regulation of the p53 network, which is also conserved at the network level but not at the level of individual miR–target pairings between human, mouse and zebrafish (Le et al., 2011). Small-RNA-seq of $tKO^{26b/a1/a2}$ cultures provided further support for this scenario. In $tKO^{26b/a1/a2}$ cultures, we noted the specific downregulation of those miRs whose expression is directly under REST control, whereas the majority of miRs were upregulated. In agreement with this, we observed elevated expression of REST-regulated miRs (miR-9, miR-124, miR-218 and miR-135a) upon transfection of miR-26 family members into WT and $tKO^{26b/a1/a2}$ cultures. Interestingly the REST-regulated miRs all have potential target sites in several REST complex members, indicating potential feedback loops for REST activity during neurogenesis. The induction of the REST-regulated miR-124 and miR-9 is sufficient to reprogram human fibroblasts into neurons (Yoo et al., 2011). Our observation that the addition of miR-124 and miR-9 mimics to NPCs did not lead to elevated miR-26 levels indicates that miR-26 is not under the control of REST and acts upstream of REST-miRs. Taken together, these findings indicate that the miR-26 family are initial regulators of REST function during early stages of neurogenesis.

Based on these findings, and in conjunction with earlier reports, we propose a model for the role of miR-26 in neurogenesis. The REST complex represses neuronal genes in ESCs and early developing cells. Although expressed, the pre-miR-26 is not active, as it is retained in the unprocessed stage (Dill et al., 2012). Upon onset of NPC-derived neurogenesis, the miR-26 family members maturate and act against *Rest* and *Ctdsp2*. This leads to reduced REST activity and, subsequently, REST-miRs start to accumulate. These miRs form a regulatory RNA network that acts against various REST components. The resulting miR-REST feedback loop ultimately leads to the inactivation of REST and the induction of neural gene expression until the cell reaches a neuronal state. In this regard it is interesting to note that the RNA helicase DDX17 controls the binding of REST to its target promoters, thereby regulating the expression of pro-neural miRs and contributing to the miR–REST axis (Lambert et al., 2018).

Our data put the miR-26 family upstream of other neuronal miRs such as miR-9 and miR-124, which is consistent with a role as initial trigger for the induction of the regulatory miR network acting in neurogenesis (Fig. 6F). Interestingly, the miR-26 family itself is known to be under tight control at the level of DICER processing. We speculate that the miR-26 family binds to a subset of protein factors that either suppress processing in non-neuronal cells or activate maturation upon transition from NPCs to NCs. Interestingly, a recent study has implicated DDX17 in miR-26a biogenesis (Lambert et al., 2018). The authors of this study found that DDX17 is required for pri-miR-26a2 processing. In contrast, our data and data from Dill et al. show that miR-26 processing is arrested during differentiation at the pre-miR-26 level – downstream from the reported role of DDX17 (Dill et al., 2012). It is hence an interesting possibility that DDX17 and another factor, yet to be identified, regulate miR-26 maturation at different levels. Recent advances in the analysis of miR-interacting proteins (Treiber et al., 2017) will help to identify and functionally characterize potential factors involved in miR-26 during neural differentiation.

MATERIALS AND METHODS

ESC culture and neural differentiation

Murine R1 ESCs (129/Sv; kind donation from Roland Naumann, Max Planck Institute of Molecular Cell Biology and Genetics, Dresden, Germany) were maintained on gelatin-coated dishes (Sarstedt) in DMEM containing 15% ESC-tested FCS (Bio & Cell), leukemia inhibitory factor (LIF)-conditioned DMEM, 100 U/ml penicillin-streptomycin, 2 mM L-glutamate, 1% non-essential amino acids, 1 mM sodium pyruvate and 0.1 mM β-mercaptoethanol. Medium was replaced daily. ESCs were split and re-plated every second day at a density of 12.5×10^3 cells/cm^2.

ESCs were differentiated into the neural lineage as described previously (Bibel et al., 2007b; Wolber et al., 2013), with slight modifications. Briefly, 3×10^6 ESCs were plated into 10 cm Petri dishes (Greiner Bio One) and cultured for 5 days under floating conditions in ESC medium with 10% FCS and without LIF to allow for the formation of embryoid bodies (EBs). To generate attached EBs, EBs in floating conditions were transferred to tissue culture dishes on day 5 and cultured in serum-free neural selection ITS-medium (DMEM/Ham's F-12, 100 U/ml penicillin-streptomycin, 2 mM L-glutamate, 5 µg/ml insulin, 50 µg/ml transferrin, 30 nM sodium selenite, 2.5 µg/ml fibronectin and 1 µM retinoic acid). After 4 days, cells were trypsinized and further cultured (1.5×10^5 cells/cm^2) on polyornithine- and laminin-coated dishes or coverslips in N2 medium (DMEM/Ham's F-12, 100 U/ml penicillin-streptomycin, 2 mM L-glutamate, 25 µg/ml insulin, 50 µg/ml transferrin, 30 nM sodium selenite, 20 nM progesterone and 100 µM putrescin). Medium was replaced 2 h and 24 h post plating. Thereafter NPCs were cultured in Neurobasal medium (Thermo Fisher Scientific), supplemented with 100 U/ml penicillin-streptomycin, 2 mM L-glutamate and 2% B27 supplement (Thermo Fisher Scientific). Medium was changed every second day. All cells were routinely tested for contamination.

Cells were cultured up to 15 days. All cells were maintained at 37°C and 5% CO_2. Media and supplements were purchased from Sigma-Aldrich if not specified otherwise.

For analysis of cumulative population doublings (CPD) of ESCs 12.5×10^3 cells/cm^2 were plated. After 48 h, total live cell numbers were determined. Subsequently, 12.5×10^3 cells/cm^2 were replated and cultured for a total of 4 passages. The population doublings (PD) at each passage were determined according to the following equation: $x=\log_{10}[\log_{10}(N_1)-\log_{10}(N_H)]$, where N_1=inoculum number, N_H=cell harvest number and x=PD (Cristofalo et al., 1998). New PD values were added to previous values to calculate CPD values. To determine cell numbers in EBs, 1×10^6 ESCs were plated onto 10 cm Petri dishes. On day 2 and day 4, EBs were trypsinized, and live cell numbers were determined.

CRISPR/Cas9-mediated KO of miR-26a1, miR26a2 and miR26b, and of miR-26 target sites

For target selection and generation of single guide RNA (sgRNA), target sequences were selected to precede a 5′-NGG protospacer-adjacent motif (PAM) using the MIT CRISPR design tool (http://crispr.mit.edu/). sgRNAs were designed so that neighboring exons and splice signals were not affected. Target site and oligonucleotide sequences are listed in Table S1. Oligonucleotides were annealed and cloned into the BbsI-linearized CRISPR/Cas9-nickase vector pX335-U6-Chimeric_BB-CBh-hSpCas9n(D10A) (Addgene 42335; deposited by Feng Zhang; Cong et al.,

Journal of Cell Science (2021) 134, jcs257535. doi:10.1242/jcs.257535

2013). First, the genomic sequences were deleted in WT R1 ESCs by transfection of a pX335-U6-Chimeric_BB-CBh-hSpCas9n(D10A) vector expressing sgRNAs specific for the deletion site using Amaxa nucleofector kit. For deletion of the entire miR-26b coding sequence, a two-sgRNA strategy was employed. For deletion of the miR-26a1 or miR-26a2 coding sequence, a four-sgRNA strategy was employed. To generate $tKO^{26b/a1/a2}$ ESCs, an ESC clone with a homozygous miR-26b deletion was transfected with vectors expressing miR-26a1 and miR-26a2 sgRNAs. For deletion of the miR-26 target site in the *Ctdsp2* 3′ UTR, a two-sgRNA strategy was employed. For the deletion of the miR-26 target site in the *Rest* 3′ UTR, a four-sgRNA strategy was employed. ESC colonies were picked and genotyped (Table S2C), and DNA sequencing of targeted loci was done to validate deletions. Additional RT-qPCR analyses for expression of pre-miRs were performed with the miR-26 KO clones to further confirm deletion of individual miR-26 family members. Proper expression of neighboring *Ctdsp* exons in miR-26 KOs were proven via RNA-seq data (for validation of miR-26 KOs see Fig. S2; for *Ctdsp2* and *Rest* miR-26 target site KO validation see Fig. S5). Two independent ESC clones for each homozygous deletion were chosen for further analyses.

miR mimic treatment

For gain-of-function studies, synthetic double-stranded RNA oligonucleotides (miR mimics) were used (Dharmacon, GE Healthcare). For transfection of NPCs on day 9 of differentiation, 3 h after plating, medium was exchanged to antibiotic-free medium with 50 nM of miR mimics and with Lipofectamine 2000 (Thermo Fisher Scientific) as transfection reagent. RNA was isolated 72 h post transfection for RT-qPCR analyses, or cells were fixed 6 days post transfection (day 15 of differentiation) for immunostaining. miR mimics were: miR mimic negative control cel-miR-67-3p mimic (CN-001000-01-05), mmu-miR-26a-5p mimic (C-310519-07-0002), mmu-miR-26b-5p mimic (C-310520-07-0002), mmu-miR-124-3p mimic (C-310391-05-0002) and mmu-miR-9-5p mimic (C-310402-07-0005). To assess unspecific effects, a control miR mimic was used based on mature *Caenorhabditis elegans* miR-67, which has a minimal sequence identity with murine miRs.

BrdU labeling

Medium was replaced with medium containing BrdU (Sigma-Aldrich) at a concentration of 10 µM on day 10 or day 12 of neural differentiation. Cells were incubated at 37°C and 5% CO_2 for 24 h. For fixation, cells were washed twice with phosphate-buffered saline (PBS), fixed using 3.7% formaldehyde (AppliChem) in PBS for 20 min and incubated with 1.5 M HCl for 30 min. After fixation, immunocytochemistry was carried out as described below.

Immunocytochemistry

Cells grown on coverslips were washed twice with PBS, fixed using 3.7% formaldehyde (AppliChem) in PBS for 20 min, permeabilized and blocked in PBS containing 0.1% Triton X-100, 0.1% Tween-20 (Sigma-Aldrich), 1% bovine serum albumin (Sigma-Aldrich) and 2% normal goat serum (Sigma-Aldrich) for 30 min. Cells were incubated with primary antibodies diluted in blocking solution overnight at 4°C. Antibodies used were: rabbit anti-Sox2 (1:500 dilution; ab97959, Abcam), rabbit anti-Map2 (1:500 dilution; ab32454, Abcam), rabbit anti-Gfap (1:500 dilution; ab7260, Abcam), mouse anti-β-III-tubulin (anti-TUBB3; 1:500 dilution; MAB1195, R&D Systems), mouse anti-nestin (1:500 dilution; 556309, PD Pharmingen), rabbit anti-Msi1 (1:500 dilution; ab52865, Abcam), and anti-BrdU (1:1000 dilution; 5292S, Cell Signaling Technology). Cyanine 2 (Cy2)- or cyanine 3 (Cy3)-labeled anti-mouse and anti-rabbit (1:200 dilution; Millipore) secondary antibodies were diluted in blocking solution and incubated (2 h, room temperature) with samples. DAPI was used to counterstain nuclei. Samples were analyzed using a confocal LSM780 microscope (Carl Zeiss) with a 20× objective. Quantifications of marked cells were done using ImageJ (NIH). Frequencies of marker-positive cells are given in relation to $DAPI^+$ nuclear signals (=100%). Fifteen random regions (850×850 µm) of every experiment were quantified.

Flow cytometry

To determine DNA content for cell cycle phase distribution analyses, propidium iodide (PI) stainings were performed. Briefly, 2×10^5 cells were washed twice with cold PBS, permeabilized (70% EtOH for 30 min at −20°C), washed with PBS and incubated for 30 min at 37°C with 10 µg/µl PI and 10 µg/µl RNase A (R5503, Sigma-Aldrich) before FACS analysis. Cell cycle distributions were determined using ModFit LT software (Verity Software House). Frequencies of apoptotic cells were determined using the PE Annexin V Apoptosis Detection Kit I (BD Biosciences). Analyses were performed on a flow cytometer (FACS Calibur, BD).

PCR analysis to detect specific transcripts, miRs and CRISPR/Cas9 deletions

Total RNA was extracted using peqGOLD RNA Pure (Peqlab). For analyses of gene expression via reverse transcription quantitative real-time PCR (RT-qPCR), 1 µg RNA was reverse transcribed using the First Strand cDNA Synthesis Kit (Thermo Fisher Scientific). Reactions were performed using ABsolute qPCR SYBR Green RT-qPCR-mix (Thermo Fisher Scientific), 100pM primer and 1 µl of template cDNA. For detection of specific miRs, cDNAs were prepared using miSCRIPT II RT Kit (Qiagen). Precursor and mature miR levels were assessed using the miSCRIPT SYBR Green PCR Kit along with miSCRIPT Primer Assays (Qiagen). Ct values were normalized to either *Gapdh*, *Rpl4* or the small nuclear RNA U6 (Qiagen) for precursor and mature miRs (Vandesompele et al., 2002). Relative gene expression levels were calculated by the $2^{-\Delta\Delta Ct}$ method. RT-qPCRs were carried out in triplicates in a Light Cycler 480 (Roche Diagnostics). To confirm CRISPR/Cas9-mediated deletion of miR-26 and miR-26 target sites, PCR analyses on genomic DNAs were performed. All primers are listed in Table S2A,B. For RNA expression analyses of mouse brains, embryos were isolated from pregnant C57BL/6J mice. Animals were obtained from the Center for Experimental Molecular Medicine (ZEMM) animal facility, Würzburg, Germany). All animal handling was done according to animal protection guidelines of the government of Unterfranken, State of Bavaria, Germany.

Cloning of luciferase reporter constructs and luciferase assay

For cloning of the luciferase reporter constructs, the 3′ UTRs of *Rest* and *Ctdsp2* were amplified using the primers listed in Table S2D with restriction sites for NotI and XhoI at their ends. The amplified 3′ UTRs were inserted in the psiCHECK2 vector (Promega). Mutations in the miR-26 target sites were introduced using the QuickChange site-directed mutagenesis kit (Stratagene) according to the manufacturer's instructions. Mutagenesis was confirmed by Sanger sequencing. For luciferase assays, 5×10^4 HEK 293T (ATCC) cells were seeded in a 24 well plate 16 h prior to transfection. Cells were co-transfected with 0.8 µg reporter construct and 50 nM miR mimics (Dharmacon, GE Healthcare) using Lipofectamine 2000 (Thermo Fisher Scientific). Medium was changed 6 h post transfection. Luciferase assays were performed 24 h after transfection using the Dual Luciferase Reporter Assay System (Promega) in a GloMax Luminometer (Promega). Firefly luciferase activity was normalized to *Renilla* luciferase activity.

Western blotting

Western blots of lysates derived from cell cultures at different time points during differentiation were incubated with primary antibodies diluted in blocking solution overnight at 4°C. Antibodies used in this study were rabbit anti-REST (1:500 dilution; ab21635, abcam), rabbit anti-CoREST (1:1000 dilution; ab32631, abcam), rabbit anti-CTDSP2 (1:1000 dilution; PA5-21624, Invitrogen), rabbit anti-SIN3a (1:2000 dilution; PA1-870, Invitrogen) and mouse anti-GAPDH (1:500 dilution; MAB 374, Merck Millipore). Secondary antibodies (HRP-conjugated goat anti-rabbit IgG, cat. no. 32460; or HRP-conjugated goat anti-mouse IgG, cat no. 32430; Thermo Fisher Scientific; both 1:2000 dilution) were diluted in blocking solution and incubated (1 h at room temperature). Quantification was performed by comparison of band intensities and normalization to loading controls using the ImageJ software (NIH).

Transcriptome analysis by RNA-seq

Total RNA from two independent clones of WT and tKO$^{26b/a1/a2}$ cell lines and two biological replicates of ESCs and NCs (day 15) were isolated using peqGold RNA pure (PeqLab). rRNA was removed using the Ribo-Zero rRNA Removal Kit (Illumina), followed by cDNA library preparation using NEB Next Ultra Directional RNA Library Prep Kit for Illumina (New England Biolabs). Sequence reads were aligned to the mouse genome (version mm10) using TopHat (Trapnell et al., 2012). Transcripts were quantified using Cufflinks and Cuffdiff, and differential expression was determined (Trapnell et al., 2012). Small RNA cDNA libraries were generated and deep sequenced as described previously (Hafner et al., 2010). Reads were mapped against murine miR annotation database (miRBase) using the Burrow–Wheeler aligner. Each miR profile was normalized to relative read frequencies (Farazi et al., 2012).

Bioinformatics and statistical analysis

Analysis of enriched GO terms was performed using the Database for Annotation, Visualization and Integrated Discovery (DAVID v6.8; https://david.ncifcrf.gov/; Huang da et al., 2009a,b). For miR target analyses, the online database TargetScan (release 7.1) was used (Agarwal et al., 2015). Data are presented as mean±s.d. for the indicated number of biological replicates (n). Data plotting and statistical analysis were done using two-tailed Student's t-test and one-way ANOVA followed by Tukey's post hoc test. Results were considered significant if: $P<0.05$ (*), $P<0.01$ (**), $P<0.005$ (***).

Acknowledgements

This article is dedicated to Albrecht M. Müller, who passed away in 2019.

The authors acknowledge the support of Heiner Schrewe, Frederic Koch, Olga Frank, Veronika Hornich and members of the DFG-funded SPP1738, as well as the helpful discussion with Ruhel Ahmad. Some of the text and figures in this paper formed part of Thomas Ziegenhals' PhD thesis that he completed in 2017 at the Graduate School of Life Sciences at the Julius-Maximilians-Universität Würzburg in the section Biomedicine.

Competing interests

The authors declare no competing or financial interests.

Author contributions

Conceptualization: M.B., U.F.; Methodology: M.S., N.W.; Software: T.Z., X.W., M.H.; Validation: M.S., N.W.; Formal analysis: M.S., N.W., X.W., M.H.; Investigation: M.S., N.W., T.Z., X.W., M.H.; Resources: M.B., U.F.; Data curation: X.W., M.H.; Writing - original draft: M.S., N.W., M.B., U.F.; Writing - review & editing: M.B., U.F.; Visualization: M.S., T.Z.; Supervision: M.H., M.B., U.F.; Project administration: M.B., U.F.; Funding acquisition: M.B., U.F.

Funding

This work was supported by Deutsche Forschungsgemeinschaft (SPP1738).

Data availability

RNA-seq data have been deposited at the NCBI GEO database under accession number GSE171727.

Peer review history

The peer review history is available online at https://journals.biologists.com/jcs/article-lookup/doi/10.1242/jcs.257535

References

Abranches, E., Silva, M., Pradier, L., Schulz, H., Hummel, O., Henrique, D. and Bekman, E. (2009). Neural differentiation of embryonic stem cells in vitro: a road map to neurogenesis in the embryo. *PLoS ONE* **4**, e6286. doi:10.1371/journal.pone.0006286

Acharya, A., Berry, D. C., Zhang, H., Jiang, Y., Jones, B. T., Hammer, R. E., Graff, J. M. and Mendell, J. T. (2019). miR-26 suppresses adipocyte progenitor differentiation and fat production by targeting Fbxl19. *Genes Dev.* **33**, 1367-1380. doi:10.1101/gad.328955.119

Agarwal, V., Bell, G. W., Nam, J. W. and Bartel, D. P. (2015). Predicting effective microRNA target sites in mammalian mRNAs. *Elife* **4**, e05005. doi:10.7554/eLife.05005

Andres, M. E., Burger, C., Peral-Rubio, M. J., Battaglioli, E., Anderson, M. E., Grimes, J., Dallman, J., Ballas, N. and Mandel, G. (1999). CoREST: a functional corepressor required for regulation of neural-specific gene expression. *Proc. Natl. Acad. Sci. USA* **96**, 9873-9878. doi:10.1073/pnas.96.17.9873

Artegiani, B., Lindemann, D. and Calegari, F. (2011). Overexpression of cdk4 and cyclinD1 triggers greater expansion of neural stem cells in the adult mouse brain. *J. Exp. Med.* **208**, 937-948. doi:10.1084/jem.20102167

Ballas, N., Grunseich, C., Lu, D. D., Speh, J. C. and Mandel, G. (2005). REST and its corepressors mediate plasticity of neuronal gene chromatin throughout neurogenesis. *Cell* **121**, 645-657. doi:10.1016/j.cell.2005.03.013

Bibel, M., Lacroix, E., Klein, C., May-Nass, R., Perez-Alcala, S., Richter, J. and Schrenk-Siemens, K. (2007a). Embryonic stem cell-derived neurons as a novel cellular model system to study neurodegenerative and neuroregenerative processes in vitro. *J. Stem. Cells Regen. Med.* **2**, 62-63.

Bibel, M., Richter, J., Lacroix, E. and Barde, Y. A. (2007b). Generation of a defined and uniform population of CNS progenitors and neurons from mouse embryonic stem cells. *Nat. Protoc.* **2**, 1034-1043. doi:10.1038/nprot.2007.147

Chen, Z. F., Paquette, A. J. and Anderson, D. J. (1998). NRSF/REST is required in vivo for repression of multiple neuronal target genes during embryogenesis. *Nat. Genet.* **20**, 136-142. doi:10.1038/2431

Conaco, C., Otto, S., Han, J. J. and Mandel, G. (2006). Reciprocal actions of REST and a microRNA promote neuronal identity. *Proc. Natl. Acad. Sci. USA* **103**, 2422-2427. doi:10.1073/pnas.0511041103

Cong, L., Ran, F. A., Cox, D., Lin, S., Barretto, R., Habib, N., Hsu, P. D., Wu, X., Jiang, W., Marraffini, L. A. et al. (2013). Multiplex genome engineering using CRISPR/Cas systems. *Science* **339**, 819-823. doi:10.1126/science.1231143

Cristofalo, V. J., Allen, R. G., Pignolo, R. J., Martin, B. G. and Beck, J. C. (1998). Relationship between donor age and the replicative lifespan of human cells in culture: a reevaluation. *Proc. Natl. Acad. Sci. USA* **95**, 10614-10619. doi:10.1073/pnas.95.18.10614

Dill, H., Linder, B., Fehr, A. and Fischer, U. (2012). Intronic miR-26b controls neuronal differentiation by repressing its host transcript, ctdsp2. *Genes Dev.* **26**, 25-30. doi:10.1101/gad.177774.111

Dinger, T. C., Eckardt, S., Choi, S. W., Camarero, G., Kurosaka, S., Hornich, V., McLaughlin, K. J. and Müller, A. M. (2008). Androgenetic embryonic stem cells form neural progenitor cells in vivo and in vitro. *Stem Cells* **26**, 1474-1483. doi:10.1634/stemcells.2007-0877

Ehses, J., Fernández-Moya, S. M., Schröger, L. and Kiebler, M. A. (2020). Synergistic regulation of Rgs4 mRNA by HuR and miR-26/RISC in neurons. *RNA Biol.* [Epub] doi:10.1080/15476286.2020.1795409

Farazi, T. A., Brown, M., Morozov, P., Ten Hoeve, J. J., Ben-Dov, I. Z., Hovestadt, V., Hafner, M., Renwick, N., Mihailović, A., Wessels, L. F. et al. (2012). Bioinformatic analysis of barcoded cDNA libraries for small RNA profiling by next-generation sequencing. *Methods* **58**, 171-187. doi:10.1016/j.ymeth.2012.07.020

Hafner, M., Landthaler, M., Burger, L., Khorshid, M., Hausser, J., Berninger, P., Rothballer, A., Ascano, M., Jr, Jungkamp, A. C., Munschauer, M. et al. (2010). Transcriptome-wide identification of RNA-binding protein and microRNA target sites by PAR-CLIP. *Cell* **141**, 129-141. doi:10.1016/j.cell.2010.03.009

Han, J., Denli, A. M. and Gage, F. H. (2012). The enemy within: intronic miR-26b represses its host gene, ctdsp2, to regulate neurogenesis. *Genes Dev.* **26**, 6-10. doi:10.1101/gad.184416.111

Huang da, W., Sherman, B. T. and Lempicki, R. A. (2009a). Bioinformatics enrichment tools: paths toward the comprehensive functional analysis of large gene lists. *Nucleic Acids Res.* **37**, 1-13. doi:10.1093/nar/gkn923

Huang da, W., Sherman, B. T. and Lempicki, R. A. (2009b). Systematic and integrative analysis of large gene lists using DAVID bioinformatics resources. *Nat. Protoc.* **4**, 44-57. doi:10.1038/nprot.2008.211

Johnson, R. and Buckley, N. J. (2009). Gene dysregulation in Huntington's disease: REST, microRNAs and beyond. *Neuromolecular Med.* **11**, 183-199. doi:10.1007/s12017-009-8063-4

Johnson, R., Zuccato, C., Belyaev, N. D., Guest, D. J., Cattaneo, E. and Buckley, N. J. (2008). A microRNA-based gene dysregulation pathway in Huntington's disease. *Neurobiol. Dis.* **29**, 438-445. doi:10.1016/j.nbd.2007.11.001

Klein, M. E., Lioy, D. T., Ma, L., Impey, S., Mandel, G. and Goodman, R. H. (2007). Homeostatic regulation of MeCP2 expression by a CREB-induced microRNA. *Nat. Neurosci.* **10**, 1513-1514. doi:10.1038/nn2010

Lambert, M. P., Terrone, S., Giraud, G., Benoit-Pilven, C., Cluet, D., Combaret, V., Mortreux, F., Auboeuf, D. and Bourgeois, C. F. (2018). The RNA helicase DDX17 controls the transcriptional activity of REST and the expression of proneural microRNAs in neuronal differentiation. *Nucleic Acids Res.* **46**, 7686-7700. doi:10.1093/nar/gky545

Lange, C., Huttner, W. B. and Calegari, F. (2009). Cdk4/cyclinD1 overexpression in neural stem cells shortens G1, delays neurogenesis, and promotes the generation and expansion of basal progenitors. *Cell Stem Cell* **5**, 320-331. doi:10.1016/j.stem.2009.05.026

Le, M. T., Shyh-Chang, N., Khaw, S. L., Chin, L., Teh, C., Tay, J., O'Day, E., Korzh, V., Yang, H., Lal, A. et al. (2011). Conserved regulation of p53 network dosage by microRNA-125b occurs through evolving miRNA-target gene pairs. *PLoS Genet.* **7**, e1002242. doi:10.1371/journal.pgen.1002242

Lim, S. and Kaldis, P. (2012). Loss of Cdk2 and Cdk4 induces a switch from proliferation to differentiation in neural stem cells. *Stem Cells* **30**, 1509-1520. doi:10.1002/stem.1114

Lu, J., He, M.-L., Wang, L., Chen, Y., Liu, X., Dong, Q., Chen, Y.-C., Peng, Y., Yao, K.-T., Kung, H.-F. et al. (2011). MiR-26a inhibits cell growth and tumorigenesis of nasopharyngeal carcinoma through repression of EZH2. *Cancer Res.* **71**, 225-233. doi:10.1158/0008-5472.CAN-10-1850

Packer, A. N., Xing, Y., Harper, S. Q., Jones, L. and Davidson, B. L. (2008). The bifunctional microRNA miR-9/miR-9* regulates REST and CoREST and is downregulated in Huntington's disease. *J. Neurosci.* **28**, 14341-14346. doi:10.1523/JNEUROSCI.2390-08.2008

Qureshi, I. A., Gokhan, S. and Mehler, M. F. (2010). REST and CoREST are transcriptional and epigenetic regulators of seminal neural fate decisions. *Cell Cycle* **9**, 4477-4486. doi:10.4161/cc.9.22.13973

Roccio, M., Schmitter, D., Knobloch, M., Okawa, Y., Sage, D. and Lutolf, M. P. (2013). Predicting stem cell fate changes by differential cell cycle progression patterns. *Development* **140**, 459-470. doi:10.1242/dev.086215

Schoenherr, C. J. and Anderson, D. J. (1995). The neuron-restrictive silencer factor (NRSF): a coordinate repressor of multiple neuron-specific genes. *Science* **267**, 1360-1363. doi:10.1126/science.7871435

Sun, Y. F., Kan, Q., Yang, Y., Zhang, Y. H., Shen, J. X., Zhang, C. and Zhou, X. Y. (2018). Knockout of microRNA-26a promotes lung development and pulmonary surfactant synthesis. *Mol. Med. Rep.* **17**, 5988-5995. doi:10.3892/mmr.2018.8602

Trapnell, C., Roberts, A., Goff, L., Pertea, G., Kim, D., Kelley, D. R., Pimentel, H., Salzberg, S. L., Rinn, J. L. and Pachter, L. (2012). Differential gene and transcript expression analysis of RNA-seq experiments with TopHat and Cufflinks. *Nat. Protoc.* **7**, 562-578. doi:10.1038/nprot.2012.016

Treiber, T., Treiber, N., Plessmann, U., Harlander, S., Daiß, J.-L., Eichner, N., Lehmann, G., Schall, K., Urlaub, H. and Meister, G. (2017). A compendium of RNA-binding proteins that regulate MicroRNA biogenesis. *Mol. Cell* **66**, 270-284.e13. doi:10.1016/j.molcel.2017.03.014

Vandesompele, J., De Preter, K., Pattyn, F., Poppe, B., Van Roy, N., De Paepe, A. and Speleman, F. (2002). Accurate normalization of real-time quantitative RT-PCR data by geometric averaging of multiple internal control genes. *Genome Biol.* **3**, RESEARCH0034. doi:10.1186/gb-2002-3-7-research0034

Visvanathan, J., Lee, S., Lee, B., Lee, J. W. and Lee, S.-K. (2007). The microRNA miR-124 antagonizes the anti-neural REST/SCP1 pathway during embryonic CNS development. *Genes Dev.* **21**, 744-749. doi:10.1101/gad.1519107

Wolber, W., Ahmad, R., Choi, S. W., Eckardt, S., McLaughlin, K. J., Schmitt, J., Geis, C., Heckmann, M., Sirén, A.-L. and Muller, A. M. (2013). Phenotype and stability of neural differentiation of androgenetic murine ES cell-derived neural progenitor cells. *Cell Med.* **5**, 29-42. doi:10.3727/215517913X666468

Wu, J. and Xie, X. (2006). Comparative sequence analysis reveals an intricate network among REST, CREB and miRNA in mediating neuronal gene expression. *Genome Biol.* **7**, R85. doi:10.1186/gb-2006-7-9-r85

Xie, L., Chen, J., Ding, Y.-M., Gui, X.-W., Wu, L.-X., Tian, S. and Wu, W. (2019). MicroRNA-26a-2 maintains stress resiliency and antidepressant efficacy by targeting the serotonergic autoreceptor HTR1A. *Biochem. Biophys. Res. Commun.* **511**, 440-446. doi:10.1016/j.bbrc.2019.02.078

Yeo, M., Lee, S. K., Lee, B., Ruiz, E. C., Pfaff, S. L. and Gill, G. N. (2005). Small CTD phosphatases function in silencing neuronal gene expression. *Science* **307**, 596-600. doi:10.1126/science.1100801

Yoo, A. S., Sun, A. X., Li, L., Shcheglovitov, A., Portmann, T., Li, Y., Lee-Messer, C., Dolmetsch, R. E., Tsien, R. W. and Crabtree, G. R. (2011). MicroRNA-mediated conversion of human fibroblasts to neurons. *Nature* **476**, 228-231. doi:10.1038/nature10323

Zhang, Y. H., Wu, L. Z., Liang, H. L., Yang, Y., Qiu, J., Kan, Q., Zhu, W., Ma, C. L. and Zhou, X. Y. (2017). Pulmonary surfactant synthesis in miRNA-26a-1/miRNA-26a-2 double knockout mice generated using the CRISPR/Cas9 system. *Am. J. Transl. Res.* **9**, 355-365.

Zhang, H., Zhang, L. and Sun, T. (2018). Cohesive regulation of neural progenitor development by microRNA miR-26, its host gene Ctdsp and target gene Emx2 in the mouse embryonic cerebral cortex. *Front. Mol. Neurosci.* **11**, 44.

Zhu, Y., Lu, Y., Zhang, Q., Liu, J.-J., Li, T.-J., Yang, J. R., Zeng, C. and Zhuang, S.-M. (2012). MicroRNA-26a/b and their host genes cooperate to inhibit the G1/S transition by activating the pRb protein. *Nucleic Acids Res.* **40**, 4615-4625. doi:10.1093/nar/gkr1278

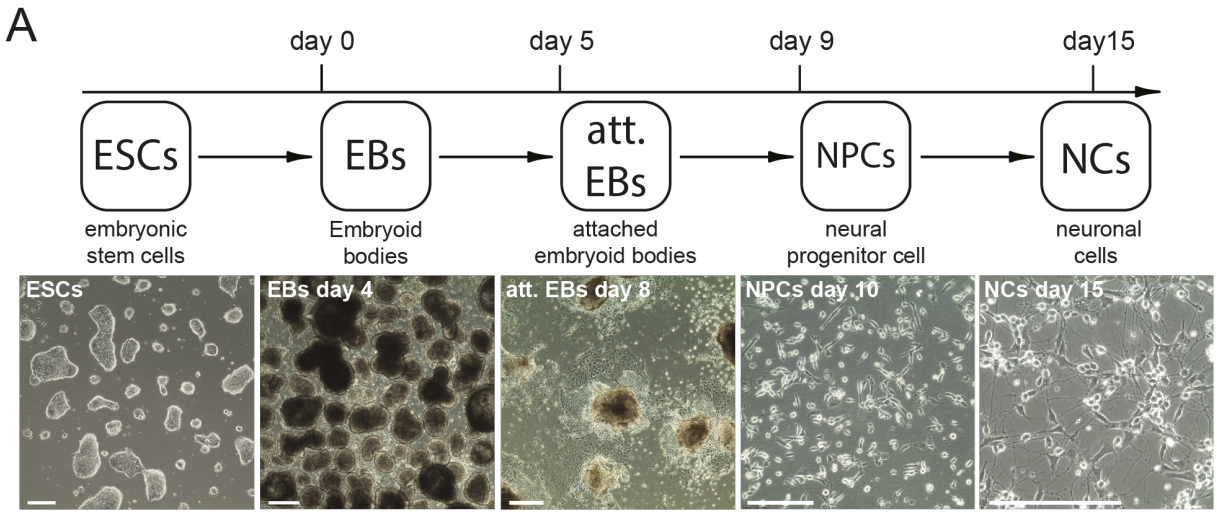

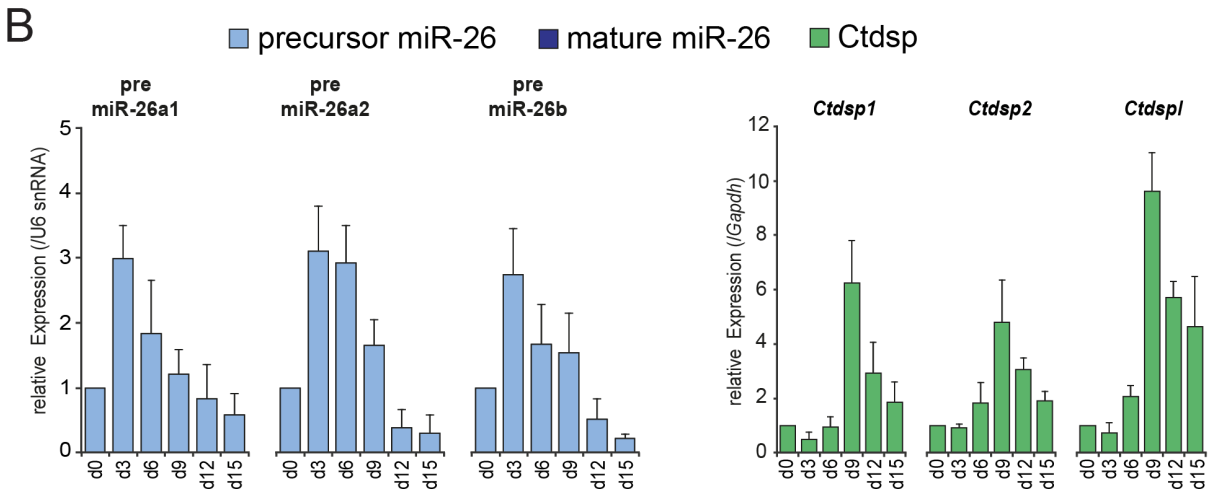

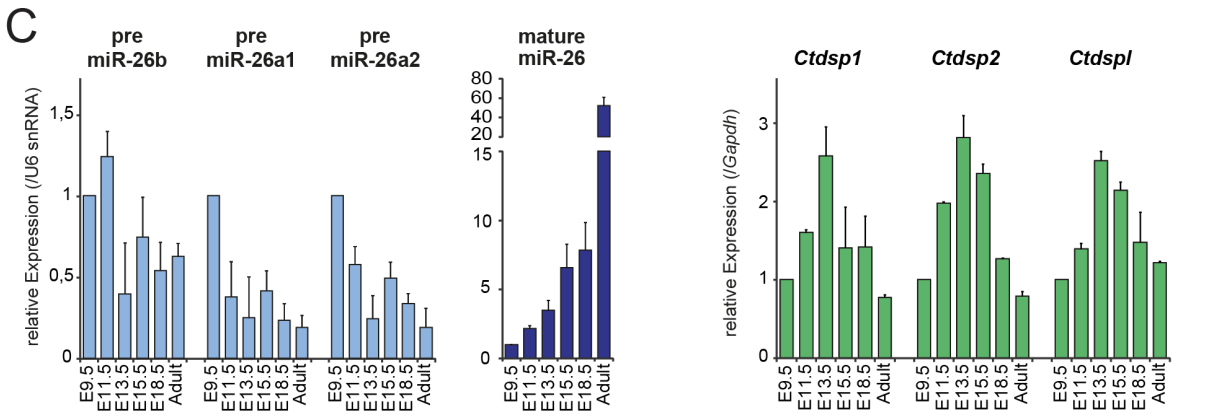

Figure S1. Expression of miR-26 family members and Ctdsp host genes in differentiating ESCs and during mouse development.

(**A**) Schematic representation of the differentiation protocol. Scale bars: 250µm (**B**) Expression pattern of pre-miR-26a1, -26a2, -26b and *Ctdsp1*, *Ctdsp2* and *CtdspL* during WT ESC differentiation. n=4 biological replicates, mean ± SD. (**C**) qRT-PCR analyses of precursor and mature miR-26 and *Ctdsp1/2/L* in the brain of mice during embryonal development and in adult brains, n = 4 biological replicates, mean ± SD.

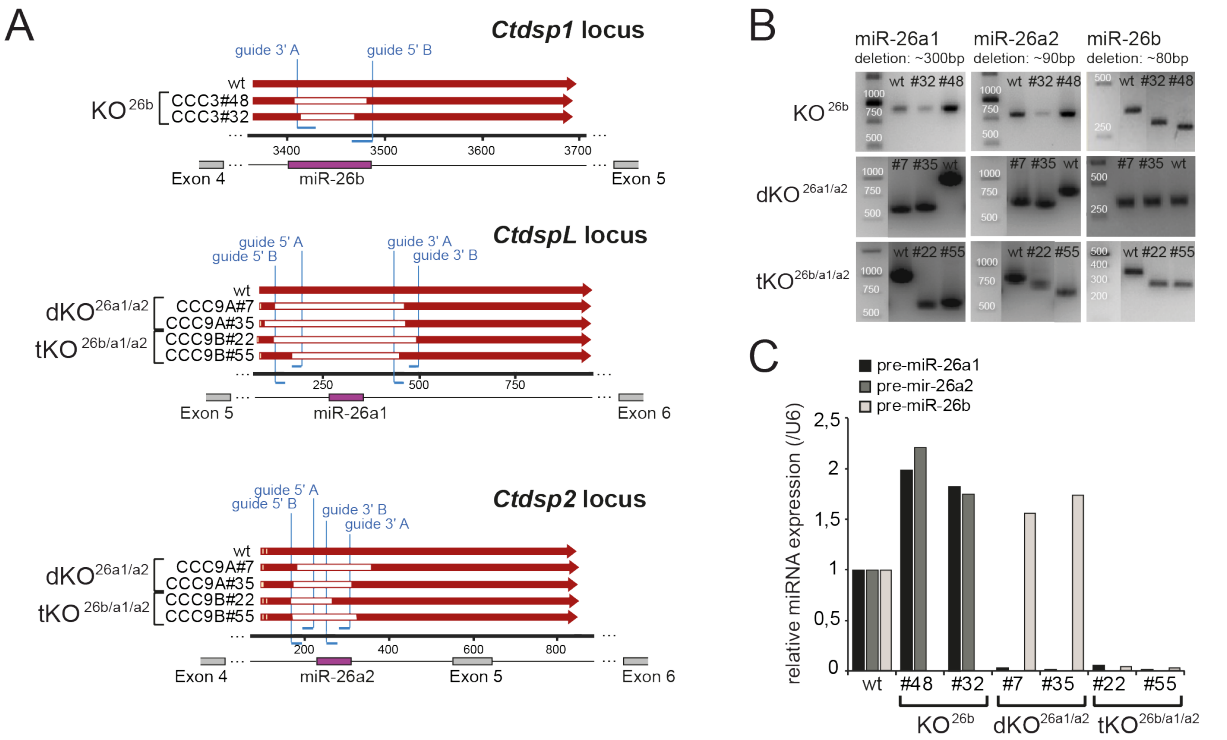

Figure S2. Generation and validation of miR-26 KO ES cell lines. (**A**) Shown are the *Ctdsp* loci, the location of miR-26 family members and the guide RNAs for Cas9-nickase deletion. WT sequences are represented by a red solid arrow, deletions by open areas. Individual ESC clone names are indicated. (**B**) miR- 26b-, miR-26a1- and miR-26a2-specific PCR analysis on genomic DNAs of WT and of miR-26 KO ESC clones. Predicted sizes of the deletions are indicated. (**C**) qRT-PCR analysis specific for pre-miR-26a1, pre-miR-26a2 and pre-miR-26b using RNA samples of WT and of KO ESCs clones. (**D**) Screen shots of *Ctdsp1*, *CtdspL* and *Ctdsp2* loci and detected reads using RNA-Seq data of WT and miR-26 KO ESC clones.

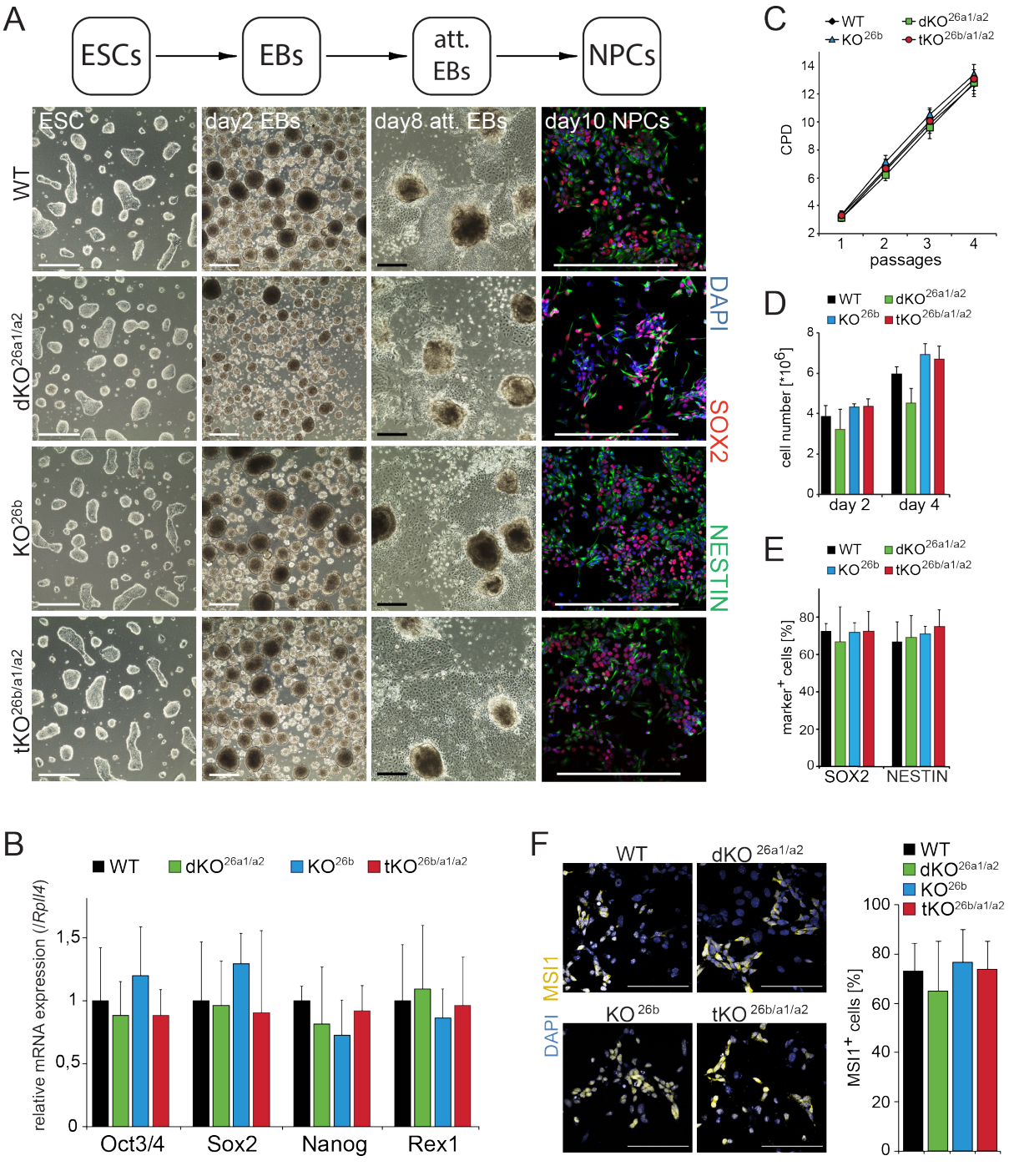

Figure S3. KO of miR-26 family members leaves differentiation of ESCs to neural progenitor cells (NPCs) unaffected. (**A**) Scheme of individual stages of *in vitro* differentiation from ESCs to NPCs (top). Phase contrast panels show representative morphological changes of WT and miR-26 KO cultures during neural differentiation from undifferentiated ESCs via embryoid bodies (EBs) to attached EBs (att. EBs). Also shown are SOX2- and NESTIN-specific immunostainings of WT, KO^{26b}, $dKO^{26a1/a2}$ and $tKO^{26b/a1/a2}$ NPC cultures (day 10, right column). Scale bars: 250µm. (**B**) qRT-PCR analysis specific for *Oct3/4*, *Sox2*, *Nanog* and *Rex1* in WT and miR-26 KO ESCs, n=3 biological replicates, mean ± SD. (**C**) Quantification of cumulative population doublings (CPD) of WT and miR-26 KO cultures ESCs throughout 4 passages (ESCs re-plated every 2nd day), n = 3 biological replicates, mean ± SD. (**D**) Single cell suspensions of WT and miR-26 KO EBs on day 2 and 4 were prepared and average cell numbers were determined (1×10^6 ESCs plated at day 0), n = 3 biological replicates, mean ± SD. (**E**) Quantification of immunostainings shown in panel A (right column). Frequencies of $SOX2^+$ and $NESTIN^+$ cells are indicated, n = 3 biological replicates, mean ± SD. (**F**) MSI1-specific immunostainings of WT and miR-26 KO NPC cultures (day 10) and their quantification (right), n = 3 biological replicates, mean ± SD. Scale bars: 100 µm.

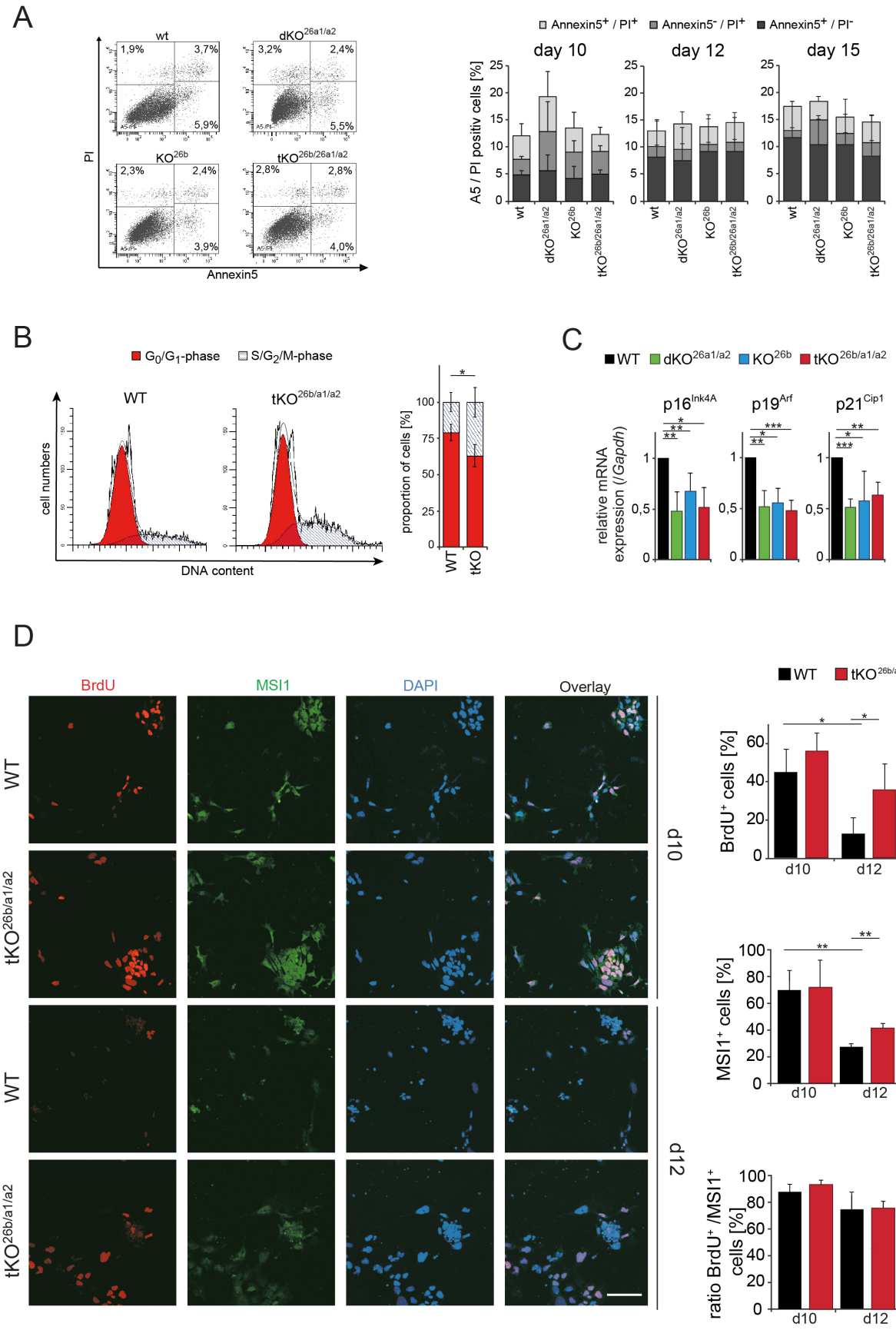

Figure S4. Apoptosis and cell cycle regulation in NPC cultures

A) Flow cytometric apoptosis and cell death analysis in WT and miR-26 KO NC cultures. Representative FACS plot (Annexin5 vs. PI) at day 15 of differentiation (left) and quantification of Annexin5- and Propidiumiodide-positive cells at day 10, 12 and 15 of differentiation (right), n = 3 biological replicates, mean ± SD. (**B**) Cell cycle phase analyses of WT and $tKO^{26b/a1/a2}$ NC cultures (day 15). The frequencies of G_0/G_1, $S/G_2/M$-type cells are shown in the bar chart (right). n=3 biological replicates, * $p < 0,05$ (t-test). (**C**) qRT-PCR analysis of the cell cycle regulators $p16^{INK4A}$, $p19^{Arf}$ and $p21^{Cip1}$ in cell cultures at day 15 of differentiation. n = 3 biological replicates, mean ± SD, * $p < 0,05$, ** $p < 0,01$, *** $p < 0,001$ (ANOVA). (**D**) Representative immunostaining of BrdU incorporation and costaining with MSI1 of cell cultures at d10 and d12 of neural differentiation. Frequencies of marker+ cell are shown on the right, n=3 biological replicates, mean ± SD. Scale bars. 100 µm, * $p < 0,05$, ** $p < 0,01$ (ANOVA).

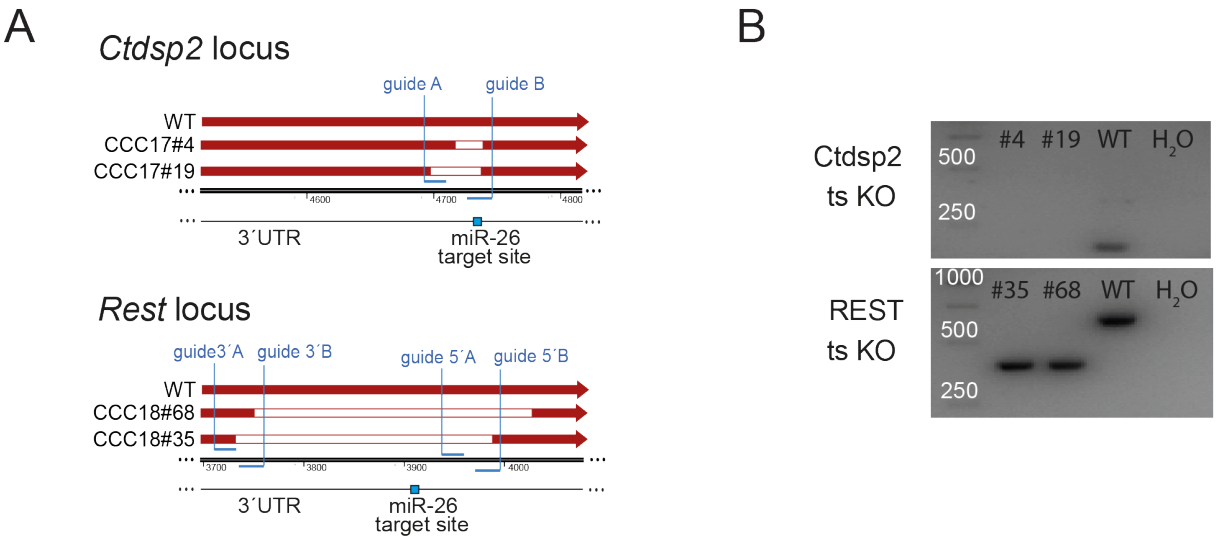

Figure S5. Generation and validation of Ctdsp2 and Rest 3`UTR miR-26 ts KO ES cell lines. (**A**) Schematic representation of the genomic Ctdsp2 and the Rest loci, the location of miR-26 target sites and the guide RNAs for Cas9-nickase deletion are indicated. WT sequences are represented by a red solid arrow, deletions by open areas. Individual ESC clone names are indicated on the left. (**B**) miR-26 target site-specific PCR analysis on genomic DNAs of WT and of miR-26 target site KO ESC clones.

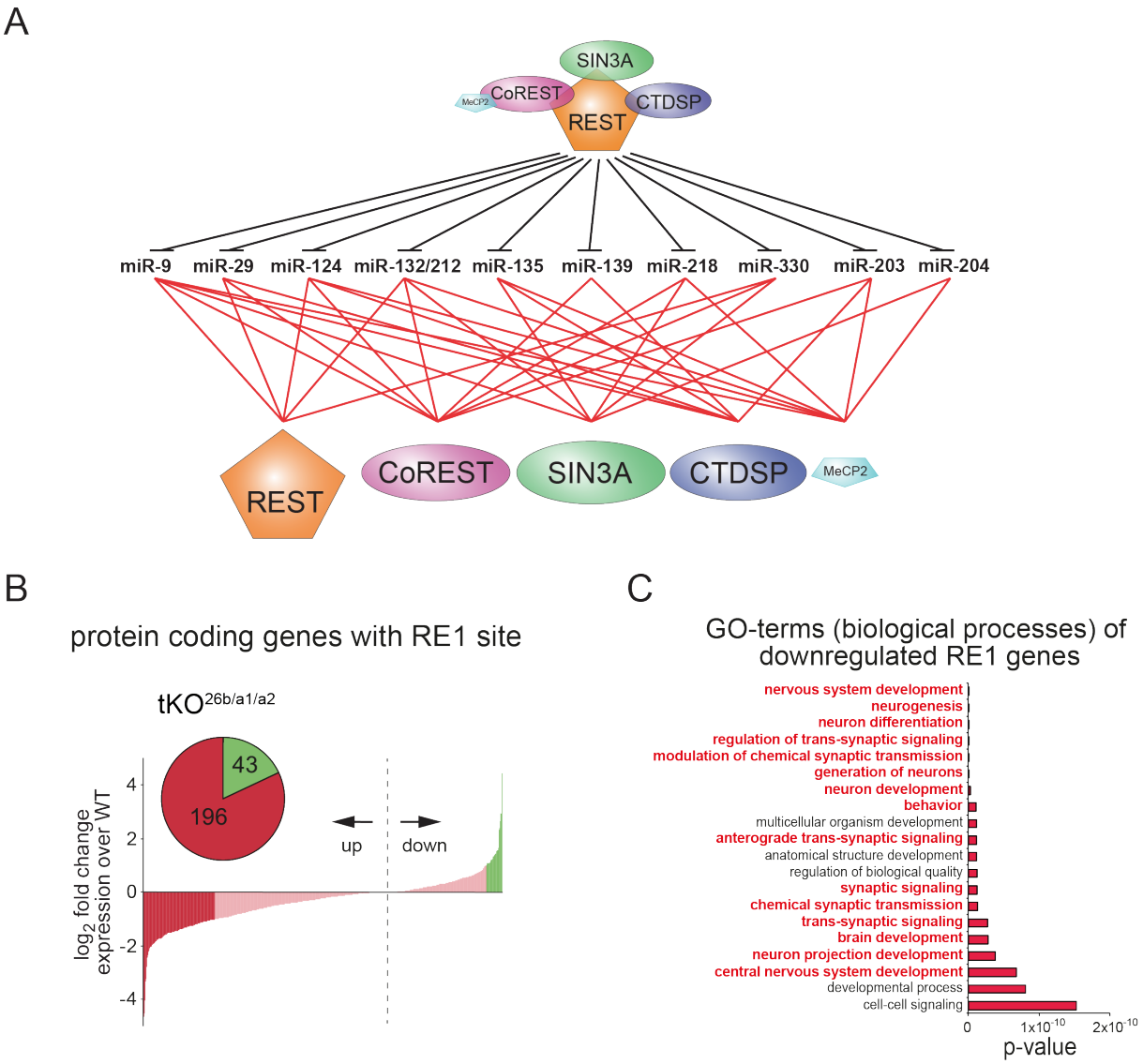

Figure S6. REST/miR network and the global downregulation of RE1 protein-coding genes in miR-26 KO cells

(**A**) Scheme of REST to miR / miR to REST regulation. REST regulated miRs and their predicted targeting to REST complex members are shown (http://www.targetscan.org/mmu_71/).

(**B**) Global down- (red) and upregulated (green) protein-coding genes with a RE1 sequence 10 kb upstream and 10 kb downstream of transcriptional start site in tKO$^{26b/a1/a2}$ cells compared to WT cells at day 15 of differentiation. Pie chart shows numbers of down- and up-regulated transcripts. (**C**) GO Term analyses of downregulated genes shown in A. No GO terms were retrieved for upregulated genes.

Table S1: Genomic target sequences and CRISPR oligonucleotides (Cas9 D10A nickase)

Name	Sequence (5' – 3'), PAM sequences underlined
miR-26b 5'A target	**GAATTACTTGAACTGGGTCCCGG**
miR26b 5'A F	CACCGAATTACTTGAACTGGGTCC
miR26b 5'A R	AAACGGACCCAGTTCAAGTAATTC
miR-26b 3'B target	**TTCTCCATTACTTGGCTCGGGGG**
miR26b 3'B F	CACCGTTCTCCATTACTTGGCTCGG
miR26b 3'B R	AAACCCGAGCCAAGTAATGGAGAAC
miR-26a1 5'A target	**CTGCACTCCGGACGTGCTTGTGG**
miR26a1 5'A F	CACCGCTGCACTCCGGACGTGCTTG
miR26a1 5'A R	AAACCAAGCACGTCCGGAGTGCAGC
miR-26a1 5'B target	**TCTTTGGCAGTAGACACCCCGGG**
miR26a1 5'B F	CACCGTCTTTGGCAGTAGACACCCC
miR26a1 5'B R	AAACGGGGTGTCTACTGCCAAAGAC
miR-26a1 3'A target	**CAAGCTTGGCTACAGGCAAAGGG**
miR26a1 3'A F	CACCGCAAGCTTGGCTACAGGCAAA
miR26a1 3'A R	AAACTTTGCCTGTAGCCAAGCTTGC
miR-26a1 3'B target	**TCCCGGAGACTCAGGACCGGAGG**
miR26a1 3'B F	CACCGTCCCGGAGACTCAGGACCGG
miR26a1 3'B R	AAACCCGGTCCTGAGTCTCCGGGAC
miR-26a2 5'A target	**CGGCTTGTGTAGGTCCCATCTGG**
miR-26a2 5'A F	CACCGCGGCTTGTGTAGGTCCCATC
miR-26a2 5'A R	AAACGATGGGACCTACACAAGCCGC
miR-26a2 5'B target	**CTGCTGGAATCCCGTACAGAAGG**
miR-26a2 5'B F	CACCGCTGCTGGAATCCCGTACAGA
miR-26a2 5'B R	AAACTCTGTACGGGATTCCAGCAGC
miR-26a2 3'A target	**TGGACGGACACAGCCTATCCTGG**
miR-26a2 3'A F	CACCGTGGACGGACACAGCCTATCC
miR-26a2 3'A R	AAACGGATAGGCTGTGTCCGTCCAC
miR-26a2 3'B target	**TCTTGATTACTTGTTTCTGGAGG**
miR-26a2 3'B F	CACCGTCTTGATTACTTGTTTCTGG
miR-26a2 5'B R	AAACCCAGAAACAAGTAATCAAGAC
Ctdsp2 A ts target	**TATCAAATCATGAAGCAAGGTGG**
Ctdsp2 A ts F	CACCGTATCAAATCATGAAGCAAGG
Ctdsp2 A ts R	AAACCCTTGCTTCATGATTTGATAC

Ctdsp2 3'B target	**TATTCAAAAACTTGAACTGTAGG**
Ctdsp2 B ts F	CACCGTATTCAAAAACTTGAACTGT
Ctdsp2 B ts R	AAACACAGTTCAAGTTTTTGAATAC
Rest ts 3´A target	**TCCTCTTACATTAACTCCCGAGG**
Rest ts 3´A F	CACCGTCCTCTTACATTAACTCCCG
Rest ts 3´A R	AAACCGGGAGTTAATGTAAGAGGAC
Rest ts 3´B target	**AGCTCGTGCAGGCAGGTGCAAGG**
Rest ts 3´B F	CACCGAGCTCGTGCAGGCAGGTGCA
Rest ts 3´B R	AAACTGCACCTGCCTGCACGAGCTC
Rest ts 5´A target	**TAACTTAATTTATATAAAGCAGG**
Rest ts 5´A F	CACCGGTAACTTAATTTATATAAAGC
Rest ts 5´A R	AAACGCTTTATATAAATTAAGTTAC
Rest ts 5´B target	**GAAAAAAAAGAGATTTTAATTGG**
Rest ts 5´A F	CACCGGAAAAAAAAGAGATTTTAAT
Rest ts 5´A R	AAACATTAAAATCTCTTTTTTTTC

Table S2: PCR oligonucleotides

A cDNA primer (qRT-PCRs)

Name	Sequence (5' - 3')
Gapdh F	TGGAGAAACCTGCCAAGTATG
Gapdh R	TCATACCAGGAAATGAGCTTGA
Rpl4 F	TTGGGTTGTATTCACTCTGCG
Rpl4 R	CAGACCAGTGCTGAGTCTTGG
Oct4 F	CCGTGAAGTTGGAGAAGGTG
Oct4 R	GAAGCGACAGATGGTGGTCT
Sox2 F	GCGGAGTGGAAACTTTTGTCC
Sox2 R	CGGGAAGCGTGTACTTATCCTT
Nanog F	TCTTCCTGGTCCCCACAG TTT
Nanog R	GCAAGAATAGTTCTCGGGATGAA
Ctdsp1 F	CCCAGTCCAGTACCTGCTTC
Ctdsp1 R	CATCTATCTCCACCGGGATG
Ctdsp2 F	GGAAGGGACCTGAGGAAAAC
Ctdsp2 R	CCTCGAAGACTGGAATCAGG
CtdspL F	GTTGAAATCGACGGAACCAT
CtdspL R	GCCAAGCTGGCAGTAAAGAG
Neurod1 F	ATGACCAAATCATACAGCGAGAG
Neurod1 R	CCAGCGACACTGAGTCCTG
Neurog1 F	CCAGCGACACTGAGTCCTG
Neurog1 R	CGGGCCATAGGTGAAGTCTT
Msi1 F	TAAAGTGCTGGCGCAATCG
Msi1 R	TCTTCGTCCGAGTGACCATCT
Pax6 F	TACCAGTGTCTACCAGCCAAT
Pax6 R	TGCACGAGTATGAGGAGGTCT
Ncam1 F	ACCACCGTCACCACTAACTCT
Ncam1 R	TGGGGCAATACTGGAGGTCA
Tubb3 F	TTCTGGTGGACTTGGAACCT
Tubb3 R	CGCACGACATCTAGGACTGA
Rest F	CATGGCCTTAACCAACGACAT
Rest R	CGACCAGGTAATCGCAGCAG
$p16^{Ink4A}$ F	GTACCCCGATTCAGGTGATG
$p16^{Ink4A}$ R	GGAGAAGGTAGTGGGGTCCT

p19^{ARF} F	GCTCTGGCTTTCGTGAACAT
p19^{ARF} R	CGAATCTGCACCGTAGTTGA
p21^{Cip} F	ACATCTCAGGGCCGAAAAC
p21^{Cip} R	GGCACTTCAGGGTTTTCTCTT

B miRNA primer (qRT-PCRs)

Name	Cat. No.:
snRNA U6	MS00033740
mmu-miR-26a-5p	MS00032613
mmu-miR-26b	MS00001344
mmu-miR-9-5p	MS00012873
mmu-miR-124-3p	MS00029211
mmu-miR-218-3p	MS00006118
mmu-miR-135a-5p	MS00011130
mmu-miR-26a-2_1_PR	MP00005250
mmu-miR-26a-1_1_PR	MP00005243
mmu-miR-26b_1_PR	MP00005257

C genomic DNA primer (Endpoint PCRs)

Name	Sequence (5’ - 3’)
miR-26b del F	GTCTTGTGCAGCCCTCTTTC
miR-26b del R	GCTTAGGGGTGATCCACAAA
miR-26a1 del F	GCGCTGGTTGTTGTGTCTAA
miR-26a1 del R	CAGTGAGAGAAGCCCTGGAG
miR-26a2 del F	CATAGACTGGGTGGCGAGTT
miR-26a2 del R	GTTTTCCTCAGGTCCCTTCC
miR-26ts-CTDSP2 F	AACTGCCCTGCACCATAAGC
miR-26ts-CTDSP2 R	TGGCATCCTACAGTTCAAGTTTT

miR-26ts-REST F	CCTCGGCAGAAGCACCG
miR-26ts-REST R	CTGTTTCAGGGGAAGGGAGATTA

D Primer for cloning luciferase reporter constructs
(lower case letters show mutation sites)

Name	Sequence (5' - 3')
Rest 3´UTR F	GATCCTCGAGCTGAGCCTCGGCAGAAGC
Rest 3´UTR R	GATCGCGGCCGCATGTTTAACTTATCCTACACAATCTTGACC
Ctdsp2 3´UTR F	GATCCTCGAGCCCATGGGTCCCTAATTAAAGAAGTTG
Ctdsp2 3´UTR R	GATCCTCGAGTGGTTGTCCCAAGTGTTGCTGATCGCGGCCG CCAGACTCTTAATGGCATCCTACAG
Rest mut 3'UTR F	ATTGGCTTAGTAAATatCTtaGAGAATTTGCCTGCTT
Rest mut 3'UTR R	AAAGCAGGCAAATTCTctAAGatATTTACTAAGCCAAT
Rest 2.mut 3´UTR F	CTAGTAACTAGTGGTAAcaTTagAATGGTAGCATTCTTTACAGC
Rest 2.mut 3´UTR R	GCTGTAAAGAATGCTACCATTctAAtgTTACCACTAGTTACTAG
Ctdsp2 mut 3'UTR F	TTGTTGTATTCAAAAcaTTagACTGTAGGATGCCATT
Ctdsp2 mut 3'UTR R	AATGGCATCCTACAGTctAAtgTTTTGAATACAACAA